

LPWAN Coverage Assessment Planning Without Explicit Knowledge of Base Station Locations

Martin Stusek^{ID}, Dmitri Moltchanov^{ID}, Member, IEEE, Pavel Masek^{ID}, Member, IEEE, Konstantin Mikhaylov^{ID}, Senior Member, IEEE, Jiri Hosek^{ID}, Senior Member, IEEE, Sergey Andreev^{ID}, Senior Member, IEEE, Yevgeni Koucheryavy^{ID}, Senior Member, IEEE, Pavel Kustarev, Otto Zeman, and Martin Roubicek

Abstract—An assessment of radio network coverage, usually in the form of a measurement campaign, is essential for multibase-station (multi-BS) network deployment and maintenance. It can be conducted by a network operator or its served consumers. However, the number of measurement points and their locations may not be known in advance for an efficient and accurate evaluation. The main goal of this study is to propose a new methodology for understanding the selection of measurement points during coverage and signal quality assessment. It is particularly tailored to multi-BS low-power wide-area network (LPWAN) deployments without explicit knowledge of BS locations. To this aim, we first conduct a large-scale measurement campaign for three popular LPWAN technologies, namely, narrowband IoT (NB-IoT), Sigfox, and LoRaWAN. Utilizing this baseline data, we develop a procedure for identifying the minimum set of measurement points for the coverage assessment with a given accuracy as well as study which interpolation algorithms produce the lowest approximation error. Our results demonstrate that a random choice of measurement points is on par with their deterministic selection. Out of the candidate interpolation algorithms, the Kriging method offers attractive performance in terms of the absolute error for NB-IoT deployments. In contrast, for Sigfox and LoRaWAN infrastructures, less complex techniques, such as the natural neighbor, linear interpolation, or inverse-distance weighting, can achieve comparable (and occasionally even better) accuracy levels.

Manuscript received March 31, 2020; revised January 11, 2021 and March 28, 2021; accepted July 21, 2021. Date of publication August 5, 2021; date of current version March 7, 2022. This work was support by the International Mobility Project MeMoV, No. CZ.02.2.69/0.0/0.0/16_027/00083710 funded by the European Union, Ministry of Education, Youth and Sports, Czech Republic, and Brno University of Technology. The work of Konstantin Mikhaylov was supported by the Academy of Finland 6G Flagship under Grant 318927. (*Corresponding author: Pavel Masek*)

Martin Stusek is with the Faculty of Electrical Engineering and Communications, Department of Telecommunications, Brno University of Technology, 61600 Brno, Czech Republic, and also with the Unit of Electrical Engineering, Tampere University, 33720 Tampere, Finland.

Dmitri Moltchanov, Sergey Andreev, and Yevgeni Koucheryavy are with the Unit of Electrical Engineering, Tampere University, 33720 Tampere, Finland (e-mail: sergey.andreev@tuni.fi).

Pavel Masek and Jiri Hosek are with the Faculty of Electrical Engineering and Communications, Department of Telecommunications, Brno University of Technology, 61600 Brno, Czech Republic (e-mail: masekpavel@vutbr.cz).

Konstantin Mikhaylov is with the Faculty of Electrical Engineering and Communications, Department of Telecommunications, Brno University of Technology, 61600 Brno, Czech Republic, and also with the Center for Wireless Communications, University of Oulu, 90570 Oulu, Finland.

Pavel Kustarev is with the Faculty of Software Engineering and Computer Systems, ITMO University, 197101 Saint Petersburg, Russia. (e-mail: kustarev@lmt.itmo.ru).

Otto Zeman and Martin Roubicek are with Vodafone Czech Republic a.s., Vodafone Business, 15500 Prague, Czech Republic.

Digital Object Identifier 10.1109/JIOT.2021.3102694

Index Terms—Accuracy, Internet of Things (IoT), location, LoRaWAN, low-power wide-area network (LPWAN), narrowband IoT (NB-IoT), measurement campaigns, multi-base-station (multi-BS), Sigfox.

I. INTRODUCTION

A. Background and Rationale

THE RECENT progress in miniaturization and automation has created a large application domain known as the Internet of Things (IoT) that has to be supported by a specific connectivity feature, named massive machine-type communication (mMTC). In response to these needs, a variety of low-power wide-area network (LPWAN) technologies, including LoRaWAN, Sigfox, and the third generation partnership project (3GPP)-ratified narrowband IoT (NB-IoT), has been proposed. From the perspective of licensing, Sigfox represents a proprietary solution, while NB-IoT and LoRaWAN are open standards supported by the 3GPP initiative and LoRaWAN Alliance, respectively, [1]–[3]. These systems are characterized by multikilometer communication ranges achieved over a relatively sparse deployment of base stations (BSs). As the range of applications includes smart home scenarios as well as industry-driven services for remote metering and sensing, radio connectivity has to be enabled in outdoor as well as deep indoor environments [4], [5].

Nonetheless, before deploying LPWAN communication technologies (which should be valid for any wireless system), radio network planning is employed to produce an initial estimate on coverage and signal quality. However, this is a complex process affected by various factors and constraints including nontechnological aspects, such as types of urban layout, legal issues, and selection of locations where the BS can be deployed. In practice, a decision on the BS placement is made based on the propagation modeling that uses 3-D city maps. Such a process may involve multiple iterations, where radio measurements are used to adjust the locations of the installation points. Even after the deployment, network operators conduct regular inspections to understand whether changes in the propagation environment have affected the coverage characteristics and the performance of their networks [6]–[8].

Our previous works [9], [10] also confirm the presence of dynamic fluctuations over extended periods of time. Two measurement campaigns conducted during several months-long intervals revealed that the fluctuations can be as high as 40 dB

in terms of the signal strength even for static deployments. These changes are not entirely random, but they are represented by a slow variation of samples oscillating around the mean value. On the other hand, microscale variations in the signal strength such as fast fading are smoothed using the “averaged” propagation models.

As a result, to maintain a relevant coverage map, the said process has to be applied periodically. The rationale is that LPWAN network operators may perform upgrades of their infrastructures or reconfigurations of the network parameters while the environmental conditions may also change with time due to, e.g., new construction in the considered area or seasonal changes. We also note that the duration of time when the propagation environment remains relatively unchanged depends on many factors and is, in general, site-specific; thus, beyond the scope of this work. Also, the coverage map update period is a valid research consideration on its own, which we leave for further studies.

On top of that, conducting a measurement campaign on the city scale is a time-consuming process. Preferably, the operators are willing to assess the network coverage and signal quality in all the available locations. One of the crucial issues in evaluating the network coverage is that the number of measurement points required for an accurate coverage and signal quality reconstruction is not straightforward to determine. In practice, it is affected by the city deployment features, selected technology, carrier frequency, etc. This problem becomes even more complex when the exact locations of the BSs are not known in advance. The latter might be the case for third-party companies aiming to purchase a service from the LPWAN operators and performing their own coverage and signal quality assessments.

The recently proposed fully automated coverage assessment techniques, such as those utilizing unmanned aerial vehicles (UAVs) [11]–[15], may be constrained either due to the weight of the measurement equipment or with respect to allowable altitudes above the ground, and may thus produce inaccurate or limited results at the evaluated points. On top of this, in some regions, the use of UAVs for such measurements may be prohibited or hampered by the legal regulations.

B. Key Contributions

In this article, we propose a new methodology for assessing the coverage and the signal quality of multi-BS LPWAN technologies. Specifically, based on the results of our extensive measurement campaign, we address the problem of signal quality estimation at the feasible points within a certain area of interest. We then quantify how the number of measurement locations affects the accuracy of estimation and how well different interpolation and thinning algorithms perform. Notably, in our study, we consider all three popular LPWAN technologies dominating the market today, namely, NB-IoT, Sigfox, and LoRaWAN. This allows us to understand how the technology features affect the coverage and the signal quality assessment procedure in city-wide LPWAN layouts.

In the first phase of this study, our joint effort with Vodafone Czech Republic¹ delivers: 1) an extensive measurement campaign for three leading LPWAN technologies publicly available today (wherein the research activities with Vodafone allowed us to adjust the network configuration as well as obtain detailed information while performing the measurement campaign), across the city of Brno located in the Czech Republic [10], [16]–[18]. Using these measurements and utilizing the knowledge of the BS locations for all the technologies in question, 2) we construct the baseline coverage map and derive a reference model used further on to characterize the prediction accuracy of the propagation models as an alternative to the interpolation methods.

In the second phase of our work, we consider exclusively the results of our practical measurements and proceed by gradually reducing the number of points taken into account randomly or deterministically, while at the same time applying appropriate interpolation techniques to 3) create reduced coverage maps. Considering the proportion of the area covered with at least a certain signal level (x dBm) and employing the weighted average metric, 4) we compare the performance of the reference model against the coverage maps produced by the interpolation algorithms. Finally, 5) we assess the performance of the reference model and the interpolation methods under thinning against the measurement results.

With the proposed methodology, one may identify the number of measurement points required to produce a coverage assessment with the desired accuracy for a city environment similar to the one of Brno, and can also deduce useful insights for other environments. In a nutshell, the main contributions of our study are follows.

- 1) We propose a methodology for identifying the number of measurement points and their locations to conduct a coverage assessment of LPWAN technologies at city scale with a given approximation error.
- 2) We show that out of a large set of the considered interpolation techniques, Kriging provides the best performance for the NB-IoT deployments, while natural-neighbor interpolation can become a viable alternative for the LoRaWAN and Sigfox deployments.
- 3) We establish that the number of measurement points required to achieve a certain coverage and signal quality assessment error increases with the density of the BSs and also depends on the communication range of the considered radio technology.
- 4) We demonstrate that a random choice of measurement points produces a similar approximation accuracy as their deterministic selection.

The remainder of this article is organized as follows. In Section II, we overview the related work. Furthermore, in Section III, the measurement campaign and the obtained results are described. Our proposed methodology for identifying the

¹Research cooperation between Vodafone Czech Republic and the Department of Telecommunications at Brno University of Technology (BUT) has started in 2017, see: [Authorized licensed use limited to: Southeast University. Downloaded on May 24,2022 at 03:16:41 UTC from IEEE Xplore. Restrictions apply.](https://www.vodafone.cz/en/about-vodafone/press-releases/message-detail/vodafone-letos-rozsviti-celonarodni-sit-pro-nb-iot/Deployment of the NB-IoT technology in Czech Republic.</p>
</div>
<div data-bbox=)

minimum sets of measurement points for an accurate characterization of the radio coverage is introduced in Section IV. The key numerical findings are summarized and discussed in Section V. Finally, the conclusions are drawn in Section VI.

II. RELATED WORK

Accurate network coverage assessment is one of the most challenging operations that precede a deployment of the end devices (EDs), which rely on wireless communications technology [19]. Field measurements provide a method of coverage characterization, but conducting these is a costly and time-consuming process. Therefore, by limiting the required number of measurement points needed to obtain accurate coverage and signal quality results, major technology adopters can save a significant amount of resources in terms of time and money.

Today, the assessment of radio coverage is even more important as many industrial companies were waiting for the 3GPP Cellular IoT (CIoT) technologies to hit the market. Therefore, the key players are now preparing their first large-scale LPWAN trials and challenge the operators to deliver a reliable network infrastructure capable of managing the massive numbers of connected devices. To the best of our knowledge, the research question of assessing large-scale deployments of multi-BS LPWAN technologies without the knowledge of BS locations has not been sufficiently investigated in the literature as of yet. In the following sections: 1) we first summarize past studies related to coverage assessment; 2) we then overview the state-of-the-art interpolation methods used for coverage estimation; and 3) we finally summarize the standard coverage assessment metrics.

A. Coverage and Signal Quality Assessment

Coverage and signal quality assessment of LPWAN technologies with explicit knowledge of BS locations was addressed in several research works. Most of these studies, however, are limited to a single channel quality indicator, i.e., reference signal received power (RSRP), received signal strength indicator (RSSI), or signal-to-interference-plus-noise ratio (SINR), thus making a comparison between different works cumbersome. Below, we report on the recent measurement setups over city-scale deployments.

Aernouts *et al.* [20] carried out an extensive measurement campaign, wherein coverage assessment data acquired for LoRaWAN and Sigfox served as an input set for the proposed localization framework. The study was conducted in the city of Antwerp, Belgium. With 84 BSs distributed over the area of 52.97 km^2 , Sigfox slightly exceeds LoRaWAN in terms of the number of gateways (GWs). For Sigfox, the authors also conducted a coverage assessment in rural environment between the cities of Antwerp and Ghent. This measurement campaign covered the total area of 1068 km^2 featuring 137 BSs. Unfortunately, there is no publicly available NB-IoT measurement trial focusing on coverage and signal quality assessment at such a large scale.

In [21], researchers characterized the distribution of long-term evolution (LTE) BSs in the city of Xian, China based on real-world measurements. The results of the conducted

measurement campaign can offer first-order insights into the density of NB-IoT BSs. In this urban scenario, 13 BSs cover the area of 3 km^2 . The density of LTE BSs in [21] is comparable with the measurement results of our work.

Some other research works employed computer simulations to estimate coverage in LPWAN systems. Lauridsen *et al.* [22] used existing Telenor's cellular deployment structure to model the coverage performance of NB-IoT, LoRaWAN, and Sigfox. The structure of the network suggested that the density of urban cells is five times higher as compared to rural areas. Furthermore, simulation results confirmed that the outages over NB-IoT and Sigfox do not exceed 1%, followed by LoRaWAN with a 2% chance of message loss.

It is essential to highlight the fact that all the aforementioned studies presume full knowledge of the BS locations. Hence, these results can be used by the operators to assess and improve their deployments. However, this approach is not suitable for third parties, which cannot directly access the BS location data.

B. Interpolation Methods

One of the crucial steps in assessing large-scale deployments is the use of prediction mechanisms to interpolate the signal quality at those points where no measurement data are readily available. Several studies followed this approach. Particularly, Akhpashev and Drozdova [23] utilized IDW interpolation to predict LTE signal quality at locations with no measurement data. However, the authors of that publication did not propose any assessment metric. Hence, the accuracy of the results cannot be verified, and the predicted value is considered as the "ground truth."

The coverage assessment in [24] employed fixed rank Kriging (FRK) to predict the signal level in the region covered by a single macrocell. The results indicated reasonable accuracy of that approach with the root-mean-square error (RMSE) ranging between 3 and 5 dB. Furthermore, the study in [21] proposed a new method of coverage map construction based on multicriteria triangulation-induced interpolation (MTI). However, that work focused only on the covered area prediction without closer specification of the expected signal levels.

Finally, Talvitie *et al.* [25] utilized linear, nearest-neighbor, and IDW interpolation schemes together with Minimum, Mean, Gradient, IDW, and nearest-neighbor extrapolation algorithms to construct their received signal strength (RSS)-based localization framework. Among all of the considered interpolation methods, Linear and IDW indicated the lowest mean error ranging from 4.3 to 8 dB. However, it should be noted that all the above research works concentrated on the signal coverage prediction incorporating a single BS. Therefore, those results are not directly comparable to the results of our study since interpolating a multi-BS coverage map is a challenging and complex task.

C. Coverage Assessment Metrics

When conducting a coverage assessment of radio network deployments, one needs to define a coverage metric. Generally, coverage quality indicators can be separated into two main

groups, namely, averaged and cumulative parameters. As an example in the first group, Liu *et al.* in [21] utilized the ratio between misclassified regions and the total area as their performance indicator. Even though this parameter allows for simple comparison of the results via a single variable, it does not provide any measure for comparing the predicted signal level accuracy. Instead, it rather focuses on the borderline values denoting the covered area.

In [25], the target metric was defined as cumulative probability of the RSS error. On top of that, the mean error as a function of the removed fingerprints was used for an initial verification of the predicted values. This metric is similar to that utilized in our work but it does not consider positive and negative deviations by using modulus. Finally, Braham *et al.* [24] defined their parameter of interest as a cumulative density function (CDF) of empirical errors between the modeled and the predicted values. Such a metric offers useful information about the distribution of error. However, it does not allow for a simple comparison of deviations as a single variable.

In our work, we combine the two approaches employed in research works [24], [25]. However, in contrast to the metric given by Braham *et al.* [24], we utilize the part of the area covered with a signal level of at least x dBm. Aside from the predicted values, it also includes the results given by the reference model. To provide an assessment metric permitting for a single-number comparison of the coverage accuracy, we further incorporate the parameter inspired by [25]. In contrast to the formula in [25], our performance indicator includes a modulus operation to account for positive as well as negative deviations.

III. OUR MEASUREMENT CAMPAIGN

To obtain the essential input data, we carried out a wide-scale measurement campaign in the city of Brno, the second-largest city of the Czech Republic. The measurement results were collected during the eight-month period between February 2019 and September 2019. The subject campaign covered over 300 unique measurement locations next to the stop stations of public transport lines (i.e., buses, trams, and trolleybuses).² The locations of the measurement points were selected to reflect one of the potential use cases of LPWAN technologies, which is localization services in Smart City applications [26].

In what follows, we offer a brief description of the selected LPWAN technologies, the measurement equipment, and the operating environment.

A. LPWAN Technologies

For our measurement campaign, we selected the three major LPWAN technologies (Sigfox, LoRaWAN, and NB-IoT) that are publicly available to the end-customers in the Czech Republic. The first two representatives: 1) Sigfox and

²The map of the measurement points in question is accessible online via https://drive.google.com/open?id=1_m9OAu4IKJqdjAy0AD1bnRBPrbbJrZ&usp=sharing Google Maps.

TABLE I
KEY PARAMETERS OF LPWAN TECHNOLOGIES

	LoRaWAN	Sigfox	NB-IoT
Coverage (MCL)	157 dB	162 dB	164 dB
Technology	PHY – Proprietary MAC – Open	Proprietary	Open LTE
Spectrum	Unlicensed	Unlicensed	Licensed
Duty cycle limitation	Yes	Yes	No
Max. EIRP	16 dBm (40 mW)	16 dBm (40 mW)	23 dBm (200 mW)
Modulation	Lora (CSS), FSK	D-BPSK (UL), GFSK (DL)	$\pi/2$ -BPSK, $\pi/4$ -QPSK, QPSK (DL + multi-tone)
Data rate in DL	0.25-11 kbps (LoRa) 50 kbps (FSK)	0.6 kbps	0.5-27.2 kbps ¹
Data rate in UL	0.25-11 kbps (LoRa) 50 kbps (FSK)	0.1 kbps	0.3-62.5 kbps ^{1,2}
Max. UL payload	242 B	12 B	1600 B ¹
Max. DL payload	242 B	8 B	1600 B ¹
TX current	45 mA	55 mA	220 mA
Sleep current	<2 uA	<2 uA	<3 uA
Battery life	10+ years	10+ years	10+ years
Module cost	6 \$	2 \$	8 \$
Security	Medium AES-128	Low ³ AES-128	Very high 3GPP (128-256 bit)

¹ The value is release-dependent (Rel. 13).

² Valid for multi-tone transmission.

³ By default, encryption is not active.

2) LoRaWAN belong to a large group of solutions operating in the license-exempt industrial, scientific, and medical (ISM) band, see Table I. Conversely, NB-IoT is one of the CIoT technologies operating in the licensed LTE band. The government regulates the utilization of both frequency ranges (in the Czech Republic, Czech Telecommunication Office is the regulator). However, the ISM conditions are much more stringent as compared with the licensed case.

1) *Sigfox*: This ultranarrowband technology is considered to be the first publicly available LPWAN solution with commercial roll-outs in 2012. The network infrastructure consists of EDs, GWs, and the cloud core. The data are transferred wirelessly to the GW and then conveyed to the cloud system via the Internet connection. The transmission of data is always initiated by the ED and can commence at any time. However, the devices cannot violate the limitation on the radio channel utilization imposed by the respective authorities. With that in mind, the uplink transmission is constrained to 140 messages per day, with the maximum size of 12 bytes. Limitations in the downlink channel are even more strict with only four messages per day having the payload of 8 bytes.

The uplink transmission is modulated with differential binary phase-shift keying (D-BPSK) having the rate of 100 bps (this value is valid for radio configuration (RC) 1 in EU, and may differ in other regions). The carrier frequency is selected randomly, typically within the 200-kHz band. Center frequency in RC 1 is set to 868.13 MHz with the maximum effective isotropic radiated power (EIRP) of 16 dBm. The reliability of data transfer is ensured by two mechanisms: 1) repetition and 2) spatial diversity. Message transmission is repeated three times, each one employing random carrier frequency selection. Furthermore, ED is not attached to a particular BS, but its data are instead received and forwarded by any of the reachable GWs [1].

2) *LoRaWAN*: The second well-known representative of the LPWAN family operating in the ISM band is LoRaWAN. Its

standard network structure is similar to that of Sigfox by comprising EDs, at least one GW, and a network server (NS). In addition, the system may feature a specialized network join (NJ) server to handle roaming between networks. In most cases, a transmission is initiated by the ED using an Aloha-like channel access mechanism [27]. It allows the ED to initiate communication at any time by not violating the operational restrictions on the selected radio channel. Within the EU region, the ED selects one of up to 16 available channels in the frequency range from 863 to 870 MHz with the bandwidth of 125 or 250 kHz. The first three channels (868.1, 868.3, and 868.5 MHz) must be supported by every ED and cannot be changed.

The ISM frequency band of 868 MHz imposes the limitation of 1% duty cycle with the maximum EIRP of 16 dBm. At the physical layer, the data are transferred with a proprietary long-range (LoRa) modulation based on the spread spectrum technique named the chirp spread spectrum (CSS). This mechanism permits LoRaWAN to operate below the noise floor. The LoRa modulation rate can be adjusted by the spreading factor (SF) parameter, which can vary from 7 to 12. The SF value controls the modulation robustness, thus directly affecting radio coverage. The achievable bitrate in the 125-kHz channel, therefore, varies from 250 (SF 12) to 5470 (SF 7) bps, which results in the maximum payload size of 51 (SF 12) up to 242 (SF 7) bytes. Due to power efficiency considerations, the static EDs are commonly configured to use the lowest SF that allows for reliable communication [2].

3) *NB-IoT*: Unlike the two LPWAN options described above, NB-IoT relates to the cellular technology operating in the licensed bands. It was introduced in 2016 as a part of the 3GPP Rel. 13 with the first commercial roll-outs in the following year [17]. The system is composed of user equipment (UE), evolved Node B (eNodeB), evolved packet core (EPC), and application servers. As the terminology suggests, NB-IoT reuses a significant fraction of the existing LTE infrastructure. In most cases, the LTE system can be upgraded to support the latest specifications via a software update [17], [28]. As compared to LTE, the bandwidth of the NB-IoT system is reduced to 180 kHz; thus, it can be deployed within a single physical resource block (PRB). On top of that, NB-IoT can operate in a stand-alone mode (a single global system for mobile communications (GSM) carrier) or in a guard band of the LTE system [28].

In contrast to LoRaWAN and Sigfox, the NB-IoT uplink operation is not based on pure Aloha but utilizes its slotted version for channel access and then resorts to using the time-frequency resources allocated by an eNodeB [27]. Since NB-IoT uses licensed frequency bands (predominantly, sub-GHz spectrum), there are no duty-cycle restrictions. The maximum uplink payload at the physical layer is 1000 bits (up to 2536 bits in Rel. 14) due to limitations on the transport block size (TBS). Furthermore, the packet data convergence protocol (PDCP) layer permits the protocol data units (PDUs) with the size of up to 1600 bytes. The transmit power of the UE can be as high as 23 dBm (there is additional support for 20 and 14 dBm power classes). In the case of a single tone uplink transmission, NB-IoT supports 15 and 3.75 kHz

subcarrier spacing with the single carrier-frequency division multiple access (SC-FDMA).

The uplink data are modulated by utilizing binary-phase shift keying ($\pi/2$ -BPSK) or quadrature phase-shift keying ($\pi/4$ -QPSK) with the continuous phase to reduce peak-to-average power ratio (PAPR). However, the highest bitrate can only be achieved with multitone transmissions utilizing QPSK modulation. If all the 12 tones are used, the theoretical throughput can be as high as 62.5 Kb/s (up to 159 Kb/s in Rel. 14). In the downlink, NB-IoT supports only 15-kHz subcarrier spacing with orthogonal frequency division multiple access (OFDMA). Furthermore, the modulation scheme is limited to QPSK with the maximum TBS of 680 bits (up to 2536 bits in Rel. 14), which results in the maximum data rate of 27.2 Kb/s (up to 127 Kb/s in Rel. 14) [3], [28]. The extended coverage (+20 dB w.r.t. LTE) is achieved primarily via repetitions. The random access channel procedure and all uplink transmissions may benefit from up to 128 repetitions [28].

B. Measurement Equipment and Setup

During our Sigfox and LoRaWAN measurements, we utilized field testers by the company Adenius. Specifically, we used ARF8121AA for Sigfox and ARF8123AA for LoRWAN. Both devices are equipped with integrated 0-dBi omnidirectional antenna and offer the theoretical communication range of 15 km. The effective radiated power (ERP) in both cases was set to 14 dBm (25 mW). When configured with SF 12 and the coding rate of 4/5, this allows to achieve the sensitivity of -137 dBm for the LoRaWAN technology. The utilized coding rate does not offer the longest communication range, but it was selected due to the requirement imposed by the LoRaWAN regional specifications [29]. For Sigfox, the standard BS SBS-T3 provides the sensitivity of up to -146 dBm [30].

In the case of NB-IoT measurements, we employed our own testing device developed at BUT. The measurement unit is equipped with SARA N210 NB-IoT module by the company uBlox. The selected module implements the NB-IoT specifications according to Rel. 13 with the maximum transmit power of 23 dBm (200 mW), thus providing the sensitivity of up to -135 dBm. The said module incorporates only one frequency band, i.e., B20 (800 MHz, uplink (832–862 MHz), downlink (791–821 MHz)), which is utilized by the Vodafone's NB-IoT network in the Czech Republic as the main frequency band [31]. On top of that, radio-wave propagation is facilitated by the omnidirectional half-wave antenna with 2-dBi gain. Specifically, it is a pentaband antenna by RF Solutions that is designated as ANT-PCB8121-FL [32].

For all the measurement points, the test devices were deployed at a selected location and positioned approximately one meter above the ground level away from buildings and other obstacles. Then, the testing units were powered up to make them transmit ten messages with the period of 30 s. To avoid interference between the LPWAN technologies, the measurement equipment was utilized sequentially. The illustrative path of a datagram for each technology is depicted in Fig. 1. The message size was set to 12 bytes for all the considered

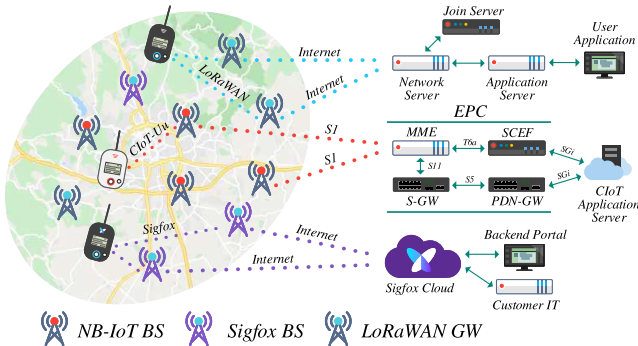


Fig. 1. Network architecture of the selected LPWAN standards.

radio technologies, to remain in-line with the limitations of the Sigfox operation, see Section III-A1. The time frames and the locations of each measurement point were recorded for further statistical analysis. The preliminary positions of the measurement points were acquired from the map and verified by Adenius testers having a built-in global navigation satellite system (GNSS) receiver.

Once the field measurements were completed, all of the available data were collected from the appropriate Web management interfaces. At the time of conducting the measurements and processing the data, only the locations of the LoRaWAN GWs were available publicly and accessible via the management interface. To acquire the locations of Sigfox and NB-IoT BSs, we had to contact the network operators Simplecell (Sigfox) and Vodafone Czech Republic (NB-IoT). In accordance with the effective agreements, the precise locations of the BSs are known to the authors and have been employed in our analysis, but they cannot be revealed publicly.

C. Data Pre-Processing

Since the NB-IoT module is always connected to a single BS, the respective data processing was a straightforward procedure. All the signal quality indicators received from a certain test location were averaged to obtain a single RSRP value, which served as an input to the subsequent interpolation methods. In the cases of Sigfox and LoRaWAN, the situation was different. The devices operating under these two technologies are not connected to a specific GW, and their messages are received by each available BS within the communication range.

In the extreme case, we observed a single packet being received by 15 LoRaWAN GWs. To acquire a single value, we selected the GW with the best average RSSI and used this result for the following interpolation methods. The points in outage were excluded from the consideration. In the last step, we used the haversine formula to obtain the distances between each measurement point and the corresponding BS/GW.

D. Measurement Environment and Network Configurations

Our measurement campaigns were executed around the city of Brno at 303 unique locations spanning over 12 km north to south and 24 km east to west. The results of these coverage measurements for each of the three LPWAN technologies

are depicted in Fig. 2. As an indicator of the coverage quality at a certain location, we utilized the RSSI values for Sigfox and LoRaWAN. Conversely, for NB-IoT, RSRP served as the primary signal quality indicator. It provides a more accurate assessment of radio channel conditions by measuring only the R0 (also R1, if available) reference signal, thus excluding the interference from other antenna sectors and unrelated channels [28]. Furthermore, RSRP is not technically available for LoRaWAN and Sigfox as these much simpler technologies do not utilize multisector antennas and reserved reference signal channels. For these reasons, the signal strength metric is limited only to RSSI, which derives the received power over the entire bandwidth.

Summarizing the processed data, all three technologies offered relatively reliable service, with only a few measurement points being in outage. The most robust connectivity was provided by the NB-IoT network—with only three unserved points—followed by Sigfox and LoRaWAN with ten and sixteen outage cases, respectively. However, these differences are marginal for the scale in question. More significant differences become visible when the signal levels are examined. For NB-IoT, the average value of RSRP was -76 dBm, whereas the mean signal levels for Sigfox and LoRaWAN were close to -100 dBm. More specifically, the values were -112 dBm for Sigfox and -98 dBm for LoRaWAN.

These differences are attributed to the features of the technologies and the densities of the BSs. With respect to the latter, the numbers of NB-IoT BSs in our test area greatly exceeded those for the two counterpart solutions. Specifically, NB-IoT is in the first place with 78 dedicated BSs having more than a quadruple volume of GWs belonging to other LPWAN solutions. In contrast, Sigfox and LoRaWAN networks only feature 13 and 19 GWs, respectively. The actual BS density also impacts the distances between the measurement points and their closest GW/BS. For NB-IoT, the average distance to the nearest BS did not exceed 0.52 km, whereas for Sigfox, it was 3.45 km and 1.86 km in the case of LoRaWAN.

IV. PROPOSED METHODOLOGY

In this section, we first outline the proposed methodology for identifying the minimum set of measurement points. Then, we proceed by specifying the reference model employed by our study as well as the considered interpolation and thinning algorithms.

A. Procedure and Metrics of Interest

The proposed procedure for identifying the minimum set of measurement points to assess the network coverage can be divided into several steps, as depicted in Fig. 3. In the first one, we utilize the knowledge of the BS locations across the area of interest and combine it with standardized propagation models to construct a reference model for each LPWAN technology.

At the second stage, we build a model without explicit knowledge of the BS locations by employing interpolation techniques to infer the RSRP (or RSSI for LoRaWAN and Sigfox) values at each point inside the considered area. To identify the minimum set of measurement points required for

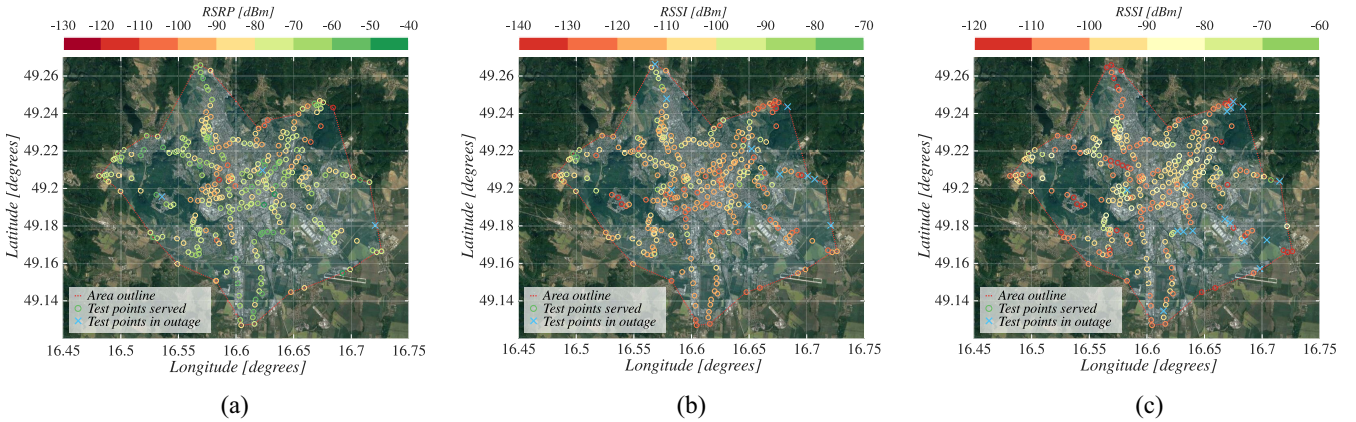


Fig. 2. Coverage of LPWAN technologies in the city of Brno. (a) NB-IoT. (b) Sigfox. (c) LoRaWAN.

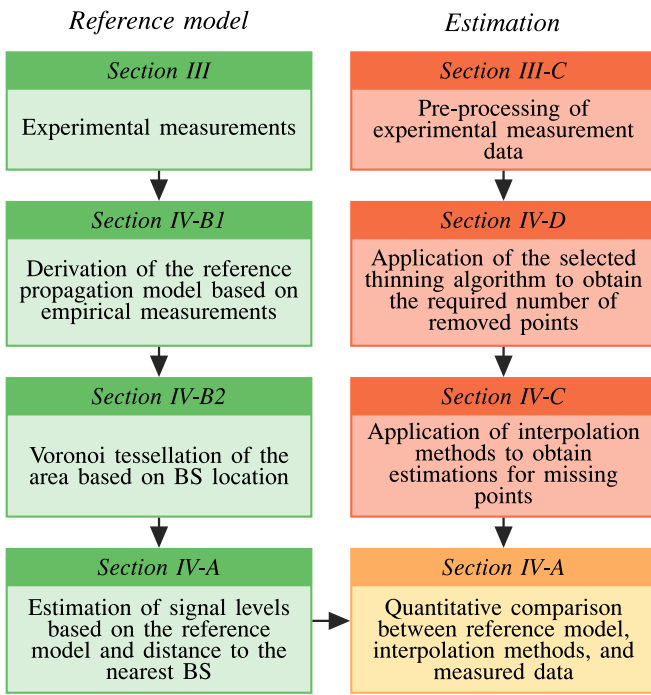


Fig. 3. Main steps of our assessment process.

accurate coverage assessment, we apply and study two fundamentally different reducing techniques, which are probabilistic and deterministic thinning.

We expect that these algorithms will significantly impact the quality of hypothesis since a random selection of measurement points should provide inferior accuracy as compared to more complex deterministic selection. Hence, we consider a range of parameters for these thinning approaches. In Section V, we also identify which one demonstrates the best performance.

For both thinning algorithms, we consecutively reduce the number of retained points. Furthermore, we apply the metrics defined below to quantitatively characterize the distance between the data set produced by the reference model (derived with the knowledge of BS locations) and the one with the reduced number of measurement points (created without the knowledge of BS locations). Finally, we compare the

prediction accuracy of the reference model and the interpolation methods against the measured values. Based on these results, we make conclusions on the minimum number of measurement points needed to provide the coverage quality assessment with a given maximum deviation from the measured values.

As a coverage assessment parameter, we employ the probability that a certain fraction of area is covered with the signal level of at least x dBm. In the sequel, we estimate this metric for both the reference model and the interpolated data by using the following approach. A regular grid with the uniform step is applied to the area of interest. The coverage quality is then estimated by using the sample values of RSRP/RSSI at each of those points. As one may observe, this parameter can be interpreted as an inverse CDF of the RSRP/RSSI values.

Note that the introduced metric allows for a convenient visual comparison between the reference model and the proposed option. However, it does not permit to quantify the distance between the two given models. To facilitate a quantitative comparison between the models, we propose the use of the mean absolute error (MAE) metric that specifies the cumulative deviation between any two models under consideration. We define this parameter as follows:

$$Q = \frac{1}{N} \sum_{i=1}^N |R_i^{(1)} - R_i^{(2)}| \quad (1)$$

where $R_i^{(1)}$ and $R_i^{(2)}$ are the sample values of the two models at the same point and N is the total number of points on the interpolation grid. Note that the modulus is used here to account for positive and negative deviations. Each point i represents one cell of the regular grid with the resolution of 50 m outlined by the area of the test locations as depicted in Fig. 2. These cells serve as an output data set of the interpolation algorithm, which estimates the RSRP/RSSI value for each point i .

As one may observe, the averaged integral metric specified in (1) is independent of the number of points N , where the coverage metric is evaluated and produces the absolute deviation from the actual coverage averaged over the total number of interpolated points N .

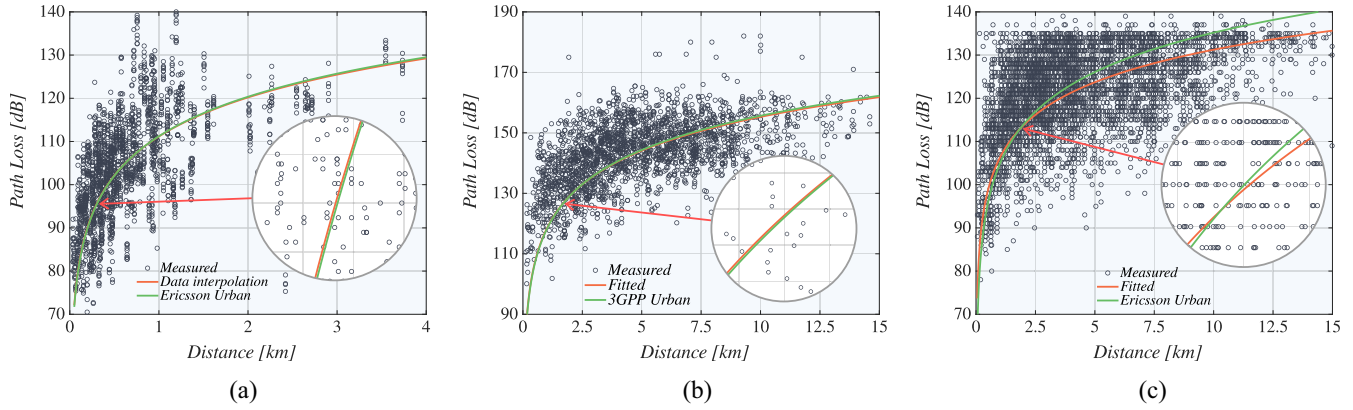


Fig. 4. Fitting of propagation model to measurement data. (a) NB-IoT. (b) Sigfox. (c) LoRaWAN.

B. Reference Model

We proceed by defining the baseline reference models for each of the considered LPWAN technologies. A reference model is intended to compare the widely used radio propagation models with the interpolation methods in terms of the prediction accuracy. Each reference model assumes that the exact BS locations are available.

1) Reference Path-Loss Model: At the first step of our modeling, we employ the measured signal levels at each location to derive the respective path-loss (PL) value as

$$\text{PL} = |P_{RX}| + \text{SNR} + P_{TX} + G; \quad P_{RX} \leq 0 \quad (2)$$

where $|P_{RX}|$ denotes the absolute value of the received signal power in dBm (RSRP in the case of NB-IoT; RSSI for Sigfox and LoRaWAN), SNR is the signal-to-noise ratio, P_{TX} represents the transmitter's effective radiated power, and G stands for the sum of antenna gains.

To derive the continuous PL curve from the discrete measurement samples, we utilize a nonlinear regression to obtain the expected coefficients of the log-distance PL model [15] as defined by

$$\text{PL} = \overline{\text{PL}}(d_0) + 10\gamma \log_{10}\left(\frac{d}{d_0}\right). \quad (3)$$

In the above, $\overline{\text{PL}}(d_0)$ represents the PL at the reference distance $d_0 = 0.1$ km, γ is the PL exponent, and d denotes the distance between the ED and the BS. The floating intercept value $\overline{\text{PL}}(d_0)$ is calculated from the free-space PL formula with an additional 10-dB attenuation capturing the propagation losses in the urban environment. The resulting fitted models together with the measured data are depicted in Fig. 4.

These empirical models derived from the measurements data characterize the city of Brno, but their accuracy may be questionable for other locations and, thus, needs to be validated. Therefore, at the second step, we select a validated PL model representing the closest match to our empirical model. During our analysis [16] of the propagation models available for LPWAN technologies, e.g., Okumura-Hata, Ericsson 9999, Stanford University Interim, and European Cooperation in Science and Technology (COST) 231 Walfisch-Ikegami, we found out that none of them provide sufficient accuracy.

TABLE II
PROPAGATION MODEL PARAMETERS [16]

Technology	Model	$\overline{\text{PL}}(d_0)$	γ
NB-IoT	Ericsson Urban	111.21	3.04
Sigfox	3GPP Urban	118.04	3.76
LoRaWAN	Ericsson Urban	104.82	3.04

Notably, the selected models in their basic form significantly overestimate the PL values for all the considered LPWAN technologies.

Therefore, we decided to utilize the propagation models from our previous work, representing the aforementioned options fine-tuned for particular communication technologies. For our approximation, we assumed 1.2-m ED height with the BS antenna 15 m above the rooftop level of 30 m and the carrier frequency of 861.7 MHz. The latter value is valid for uplink NB-IoT operation in the guard-band mode within band 20 (800 MHz), which is utilized by Vodafone's network in the Czech Republic. For other LPWAN technologies, we imply the frequency of 868.1 MHz. This value is close to the center uplink frequency used by Sigfox and corresponds to the first channel of LoRaWAN.

The subject fine-tuned models were cross-validated with the measurement data in two cities. Hence, it is expected that their accuracy will be sufficient in the case of a typical midsize European town. As it is depicted in Fig. 4, both NB-IoT and LoRaWAN are most accurately represented by the Ericsson Urban model, whereas 3GPP Urban captures Sigfox the best. The parameters of each propagation model are given in Table II.

Both models are best suited for urban and suburban environments outside the high-rise core, where the buildings have a near-uniform height. This description characterizes the city of Brno well, as its urban layout primarily comprises of mid-rise buildings. More precisely, the Ericsson Urban model is applicable for frequencies up to 1900 MHz, BS heights ranging from 20 to 200 m, ED heights between 1 and 5 m, with BS-ED separation distances up to 100 km. The 3GPP Urban model can be used for frequencies of up to 2600 MHz, with a cell radius less than 8 km and BS antenna height of up to 50 m above the average rooftop level [33].

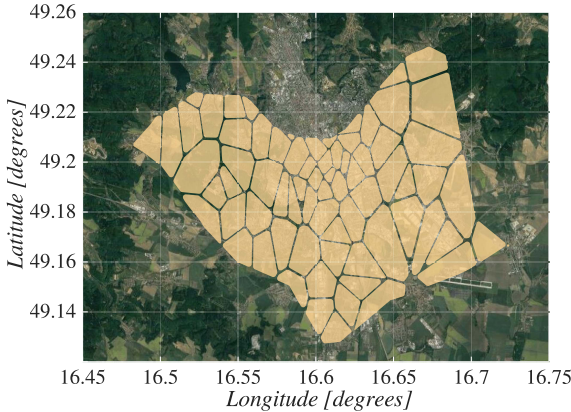


Fig. 5. Voronoi tessellation of NB-IoT deployment.

2) *Voronoi Tessellation*: The next step of the reference model derivation concerns the Voronoi tessellation. Its primary purpose is to divide the area covered by the BSs into the corresponding regions that consist of all the points on the plane closer to the seed (BS) than to any other. In other words, Voronoi tessellation dissects the area into polygons with the BS located inside representing the closest BS for all the points in that polygon. The outcome of the Voronoi tessellation process for NB-IoT technology is depicted in Fig. 5. A similar tessellation procedure is repeated for Sigfox and LoRaWAN BS locations.

Finally, the radio propagation models derived in the previous step are applied to the tessellated area to specify the expected signal level at each point of interest. These points are defined by a regular grid with 50-m resolution, thus creating the baseline coverage models. In what follows, these constructs are named the “reference” models. It is worth noting that these reference models have been derived with the exact knowledge of BS locations and then compared against the models generated using the interpolation methods, which were constructed using only the measurement data.

At this point, it is crucial to highlight that the reference model was not used to exclusively quantify the accuracy of the results. We do not consider the constructed reference model to be the so-called “ground truth” for a comparison with the proposed interpolations-based approach. Therefore, the presented results should be considered as a comparison of the two models rather than a comparison of the “ground truth” with the results of the proposed methodology.

C. Interpolation Algorithms

Fig. 2 indicates that our measurement data does not spread densely across the entire area. Therefore, to predict the service quality at all the points of the regular grid, one may resort to the use of interpolation methods. Since the measurement locations are not spread evenly, we exclusively consider the interpolation methods for scattered data. In our work, we select five most common representatives that can interpolate the arbitrarily spaced data. The chosen algorithms cover the entire spectrum of complexity from simpler and more straightforward, such as: 1) nearest-neighbor interpolation, to

the schemes with intermediate complexity, including 2) linear, 3) natural-neighbor, and 4) IDW approaches, to more computationally demanding, e.g., 5) the Kriging algorithm.

1) *Nearest-Neighbor*: This method is a simple approach to data interpolation. The initial step is the Delaunay triangulation of known points x . Then, the vertices are lifted by the magnitude of V into the dimension orthogonal to x . The same lifting procedure is also conducted for the requested point x_q . In general, this involves traversing the triangulation data structure to find the triangle enclosing the requested point. Once that position is established, the closest known point value is reused in the requested point x_q [34], [35].

The main advantage of this method is its simplicity and low computational cost. On the other hand, the resultant interpolation does not create new values for the requested points but rather duplicates the existing ones. This leads to formation of sharp transitions at the edges of the neighboring cells [35].

2) *Linear*: The main idea of Linear interpolation is equivalent to that of the Nearest-neighbor method [34]. The area defined by the measurement points is tessellated with Delaunay triangulation, and the vertices are lifted orthogonally to the known points x by the magnitude of V . However, the value of the requested point x_q is not duplicated from the closest known point but is rather calculated as the weighted sum of the magnitudes of the three vertices that constitute the enclosing triangle.

Linear interpolation utilizes the Barycentric coordinate system [36] to overcome the problem of value prediction where the points lie directly on the connecting lines of vertices. If the requested point x_q is placed inside the triangle and is connected to each vertex, the resulting diagram consists of three separate triangles with the areas of A_1 , A_2 , and A_3 . If A denotes the area of the original triangle, one can calculate the Barycentric coordinates α , β , and γ [37] as

$$\alpha = \frac{A_1}{A}, \quad \beta = \frac{A_2}{A}, \quad \gamma = \frac{A_3}{A}. \quad (4)$$

The sum of these coordinates is always equal to one; therefore, it is possible to calculate the third coordinate by subtracting the sum of the first two from unity. The resulting value of the interpolated point x_q is produced as

$$x_q = \alpha V_A + \beta V_B + \gamma V_C \quad (5)$$

where V_A , V_B , and V_C represent the vertices of the triangle.

The main benefit of this interpolation method is its speed (considerably slower than Nearest-neighbor though) and ease of implementation. However, linear interpolation only provides C^0 smoothness [35].

3) *Natural-Neighbor*: The essence of natural-neighbor interpolation is a Voronoi diagram structure. In the initial step, the known points are used to tessellate the covered area. Each cell of such a diagram contains one generating sample point that defines the value for the entire cell. Voronoi tessellation is discontinuous by its nature, but it has useful characteristics that natural-neighbor interpolation utilizes. Here, each edge represents a link between two generating sample points. This property is used to select the corresponding neighbors for the interpolation [38].

The next step in the interpolation process is point insertion. The requested point x_q is inserted into the Voronoi diagram, and a new polygon generated by the requested point x_q is added to the structure. Consequently, a part of the area from the neighboring cells is transferred to thus inserted polygon, and some edges covered by the new cell are subsumed. The main goal of the next step is to identify the weights of the neighboring samples and combine them with the sample values to obtain an estimate of the requested point x_q . Hence, each of the neighboring cells contributes a certain fraction of its area to the new cell.

Furthermore, the value of the requested point x_q is computed as the weighted average of the surrounding sample polygons. This approach is similar to that in linear interpolation but the mean is not limited to three vertices of the enclosing triangle. The fractional contribution of each polygon λ_i can be written as

$$\lambda_i = \frac{A_i}{A} \quad (6)$$

where A_i is the area of the contributing cell i and A is the total area of the inserted polygon. The sum of these weights is always one. Finally, the interpolated value is calculated as

$$x_q = \sum_{i=0}^N \lambda_i \cdot z_i \quad (7)$$

where N is the number of neighbors surrounding the inserted polygon, λ_i is the weight of each element, see (6), and z_i is the value of the sample point [39].

The key advantages of this interpolation method lie in its relative simplicity, speed, and resilience to biases introduced by how the samples may cluster. One of the drawbacks though is the slope discontinuity; therefore, it cannot offer C^1 continuity over the entire surface [38], [39].

4) IDW: The main premise of IDW interpolation is in that the values of more proximate points are related closer than for the farther away ones. In other words, the interpolated values are calculated by using a linearly weighted combination of the sample point sets. The weight is defined as an inverse function of distance. The value of the requested point x_q is calculated as

$$x_q = \frac{\sum_{i=0}^n d_i^{-p} \cdot z_i}{\sum_{i=0}^n d_i^{-p}} \quad (8)$$

where z_i is the value of the sample point, d_i is the distance between the requested and the sample points, and p is the power parameter [40]. The latter controls the significance of the known point x for the interpolated value based on its distance to the requested point x_q .

Hence, the closest points have the most significance for the resulting value of the requested point. The power value is not defined strictly and does not have connection to the real-world process. The typical convention here is to use the power of two, which we also employed in this work. Finally, the value of n determines the number of samples for interpolation and may be up to the total number of points in the data set (typically three or more though).

The selection of input sample points significantly impacts the behavior of the interpolated surface. Along these lines, IDW offers immense variability as it can use, e.g., a fixed

search radius where the requested value is calculated from the points at the preset maximum distance. Furthermore, the shape of the search window does not have to be a circle. Another option is the variable radius, where the search window is defined by the number of neighboring points used for calculation. In this work, we follow the latter approach, where the requested value x_q is derived from the five closest points [41].

IDW is an intuitive, easy to understand, and computationally efficient interpolation method. However, its accuracy decreases if the sample points are not distributed evenly. Also, the resulting surface does not provide C^1 smoothness. Moreover, the selection of input parameters is entirely arbitrary but it influences the resulting interpolation surface drastically [40].

5) Kriging: This interpolation algorithm belongs to the class of geostatistical methods based on statistical models that incorporate autocorrelation (in the sense of mathematical relationship between the measured points). Hence, geostatistical techniques have the capability of producing a prediction surface, and also offer an assessment of the interpolation accuracy. Kriging accuracy is the highest when there is a spatially correlated distance or directional bias in the input data [42].

Producing interpolated values is similar to how it is done by natural-neighbor or IDW according to (7). However, the process of weight derivation differs drastically. Kriging weights are based not only on the distance to the sample point but also on the overall spatial arrangement of the measurement points. To achieve this, Kriging follows a two-step process as it: 1) creates a covariogram and covariance functions and 2) predicts unknown values.

The initial step of the Kriging procedure is in designing an experimental semivariogram [43], which is given as

$$\gamma(h) = \frac{1}{2N(h)} \sum_{i=1}^{N(h)} [z(x_i) - z(x_i + h)]^2 \quad (9)$$

where $N(h)$ is the number of pairs that are separated by the distance of h and $z(x_i)$ is the value of the input point. The experimental semivariogram is then fitted to the empirical semivariogram. This step is needed because the experimental semivariogram is not a continuous function but is rather represented by a set of points. For our work, we employ the spherical semivariogram, which is defined as

$$\gamma(h) = \begin{cases} c_0 + c_1 \left[\frac{3h}{2a} - \frac{1}{2} \left(\frac{h}{a} \right)^3 \right] & \text{for } 0 < h < a \\ c_0 + c_1 & \text{for } h \geq a \end{cases} \quad (10)$$

where a is the range, c_0 is the nugget variance, and $c_0 + c_1$ is the sill. Selection of semivariogram impacts prediction of unknown values. Therefore, it is necessary to choose a model that fits sample data the best. The last step of the Kriging process is prediction of the requested points. In our work, we use Ordinary Kriging but there are other variants of the prediction process [44]. For Ordinary Kriging, the system is produced as

$$\begin{bmatrix} \lambda_1 \\ \vdots \\ \lambda_n \\ \mu \end{bmatrix} = \begin{bmatrix} C_{11} & \cdots & C_{1n} & 1 \\ \vdots & \ddots & \vdots & \vdots \\ C_{n1} & \cdots & C_{nn} & 1 \\ 1 & \cdots & 1 & 0 \end{bmatrix}^{-1} \begin{bmatrix} C_{10} \\ \vdots \\ C_{n0} \\ 1 \end{bmatrix} \quad (11)$$

where μ is the Lagrange parameter and C_{1n} is the covariance between the locations of sample points x_1 and x_n . The latter is computed as

$$C_{1n} = \text{Cov}(x_1 - x_n) = C(0) - \gamma(x_1 - x_n) \quad (12)$$

where $C(0)$ is the sill of the semivariogram model and γ is the value generated by the semivariogram model for the vector joining the points x_1 and x_n . The weights λ_n are then used to predict the value of the requested point x_q according to (7).

The key strength of Kriging over other deterministic methods is in that the information about spatial relationships is readily included into the weight calculation. On the other hand, Ordinary Kriging is computationally demanding; particularly, the calculation of sample weights is a time-consuming process.

D. Thinning Algorithms

The minimum set of measurement points providing the quality assessment with a given accuracy theoretically depends on the way how these points are chosen. In our study, we thus consider two fundamentally different techniques.

1) *Probabilistic Thinning*: Probabilistic thinning is a simple approach, which has an important feature that it straightforwardly translates into the choice of the measurement points when planning a measurement campaign. In probabilistic thinning, the choice of the points to be removed is made randomly and independently of each other.

2) *Deterministic Thinning*: An alternative coverage assessment is provided when the measurement points are spread densely and equally over the entire area. Hence, deterministic thinning ensures that for a given number of retained measurement locations, these reside as far from each other as possible. To determine the structure of the measurement points from a random field, we use the following approach: 1) define an $M \times M$ grid that specifies squares on the coverage map; 2) estimate the number of points in each resulting square and sort them in the descending order; 3) determine how many points need to be removed, e.g., 10%; 4) remove the measurement points from the square having the highest number of points, such that the number of points therein equals the number of points in the cluster having the second-highest number of points; 5) keep removing points from the two clusters having the highest numbers of points until when the numbers of points in those equals the number of points in the cluster having the third-highest number of points; and 6) continue until the required number of points has been removed.

For all the considered interpolation techniques, we employ a similar procedure to identify the set of measurement points that characterize the coverage quality with a certain deviation. Particularly, at each step, we remove 10% of points and then estimate the coverage-related metrics. Note that the latter approach is deterministic only on the $M \times M$ grid level. The points in each cluster are removed randomly; therefore, the nature of removing points from the individual clusters is probabilistic.

In contrast, the former method is inherently random. It is worth mentioning that the thinning is also connected with the addition of an artificial point to each corner of the interpolated

area. Without this step, an extrapolation procedure has to be applied, which we aim to avoid. To this end, the value is set to the minimum sensitivity of each LPWAN technology (signal level of around -140 dBm). However, to reduce the impact of the artificial points on the interpolation procedure, we limit their use as much as possible. These points are currently inserted into the input data set only when the area bounded by the measurement points cannot be fully interpolated (i.e., interpolation returns undefined values). This approach has proven to be reliable when the interpolation is influenced only in the extreme cases of removed points (more than 97%).

V. NUMERICAL RESULTS

In this section, we provide the numerical results and evaluate the considered coverage assessment strategies. Recall that our goal is to assess the accuracy of the proposed algorithm for different densities of measurement points in the environment, where the BS locations remain unknown, thus reflecting the precision versus time consumption tradeoff. To this aim, we start by constructing the reference coverage and the signal quality assessment models described in Section IV-B. We then proceed with selecting the appropriate interpolation tools out of those introduced in Section IV-C.

Furthermore, we compare the performance of thinning algorithms specified in Section IV-D. The presented results should be treated as a comparison of the two models rather than a comparison of the reference model with the results of the proposed methodology. Then, we report on the coverage assessment accuracy with respect to the MAE metric defined in Section IV-A. We continue by summarizing our insights in the form of a lower bound on the number of measurement points required to deliver accurate coverage assessment. Finally, the section concludes with an accuracy assessment of the proposed models with the measured results, i.e., the correlation between the reference model (“ground-truth” data), the predicted values, and the measured data.

A. Comparison of Interpolation Methods

Before assessing radio coverage and signal quality with a limited number of measurement points as well as comparing the performance of thinning algorithms, we analyze the considered interpolation methods with the goal of selecting the algorithms offering the best performance. To this end, we apply the candidate interpolation methods for the scattered input data set to estimate the signal values on a regularly spaced grid. The performance of the interpolation methods is directly compared against the reference model by using the metrics defined in Section IV-A, i.e., inverse CDF and integral MAE parameter (1).

Concerning the CDF values, Fig. 6 offers a visual comparison between the considered interpolation methods and the reference models for all three LPWAN technologies, i.e., NB-IoT, Sigfox, and LoRaWAN, by relying on the cumulative percentage of the area featuring the RSRP/RSSI level of at least x dBm as the parameter of interest. As one may observe, none of the considered interpolation tools provide a perfect fit. However, some methods are significantly better than the

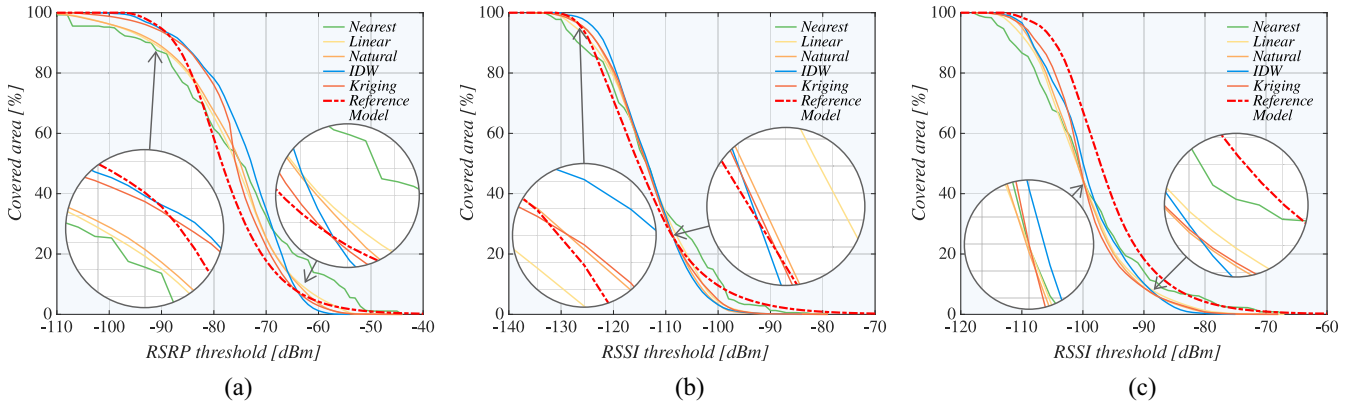


Fig. 6. Comparing interpolation methods with reference model. (a) NB-IoT. (b) Sigfox. (c) LoRaWAN.

other. Notably, the Nearest-neighbor algorithm demonstrates the largest deviation from the reference model out of all the selected interpolation techniques; it is characterized by a sharp decline in the regions of small and high values of RSRP/RSSI.

On the contrary, in the case of NB-IoT, the IDW algorithm offers the worst approximation in the area around the median of the data. It has to also be noted that for NB-IoT, the individual interpolation methods differ from each other most significantly. Two primary facts cause this phenomenon. First, the BS density in the NB-IoT deployment is considerably higher than that for the Sigfox and LoRaWAN layouts, thus influencing the reference model as well as the CDF curve's steepness. Second, the majority of the measurement points oscillate on a short-range scale around the RSRP value of -75 dBm. Hence, the remaining values need to be interpolated from a lower number of samples. For Sigfox and LoRaWAN, the rest of the algorithms display similar outputs.

To numerically quantify the performance of the considered interpolation algorithms, Fig. 7 delivers a comparison with the reference models by using the integral coverage metric defined in (1). Recall that this parameter can be interpreted as a deviation of the coverage metric (RSRP/RSSI) averaged over the set of selected interpolated points. As one may observe, the above conclusions are confirmed numerically. Particularly, the Nearest-neighbor algorithm is characterized by the worst performance out of all the considered interpolation methods.

Even though the IDW option is the second-worst for NB-IoT, its results exhibit the lowest deviation in the cases of Sigfox and LoRaWAN technologies. Contrarily, the Kriging algorithm performs as the second-worst for Sigfox and LoRaWAN, whereas in the case of NB-IoT, it is the most reliable option. The remaining linear and natural interpolation methods provide satisfactory results for all three considered LPWAN technologies, with natural interpolation providing a slightly smaller deviation. Surprisingly, all the subject algorithms display comparable results even though their approaches to the interpolated values derivation differ significantly.

Another important observation is that the quality of the resultant approximation heavily depends on the BS deployment density. Analyzing the data presented in Fig. 7, we note that the highest MAE deviation is observed for the

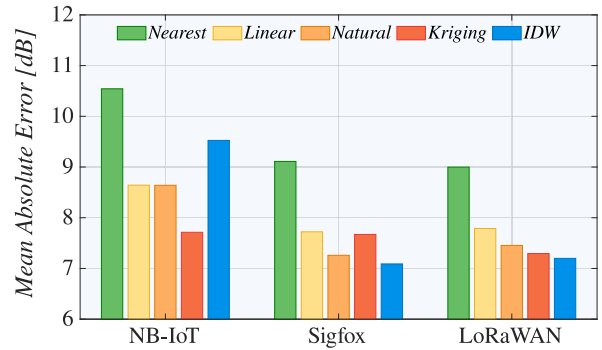


Fig. 7. Mean deviation for interpolation methods.

NB-IoT technology. At the same time, the output for Sigfox and LoRaWAN is noticeably better—this behavior confirms the visual observation gained from Fig. 6. In the considered case, NB-IoT is associated with the densest deployment, while Sigfox relies upon the smallest number of BSs located within the area of interest. We finally note that the averaged deviation as per (1) for the reference model is around 8.5 dB for NB-IoT and approximately 7.4 dB for Sigfox and LoRaWAN. Hence, one may conclude that the quality of the approximation degrades as the BS deployment density grows.

B. Comparison of Models Under Thinning

In our approach, we target dynamic environments with locations having diverse propagation conditions, where even the use of a precisely fine-tuned model may deliver inaccurate output data. Therefore, the presented results should be considered as a comparison of the two models rather than a performance comparison of the so-called “ground truth” (reference model) with the results of our proposed methodology. To do so, we proceed with contrasting the interpolation algorithms for the thinned data set with a certain fraction of points removed according to the algorithms outlined in Section IV-D. We aim to assess whether the performance of the selected interpolation algorithms degrades, and if so, how rapidly this occurs under different percentages of excluded measurement points as the interpolation mechanisms should reflect the changes more precisely.

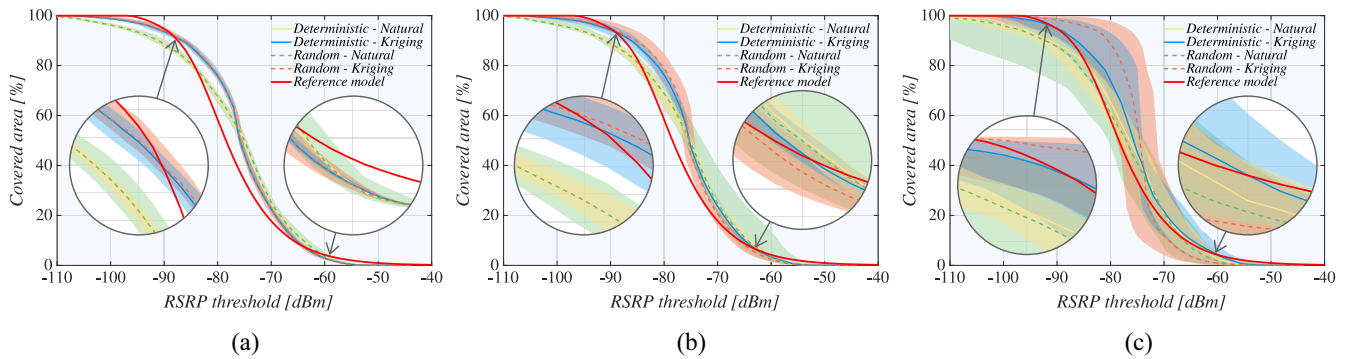


Fig. 8. Performance comparison of interpolation methods and thinning algorithms for NB-IoT. (a) 10% of removed points. (b) 30% of removed points. (c) 70% of removed points.

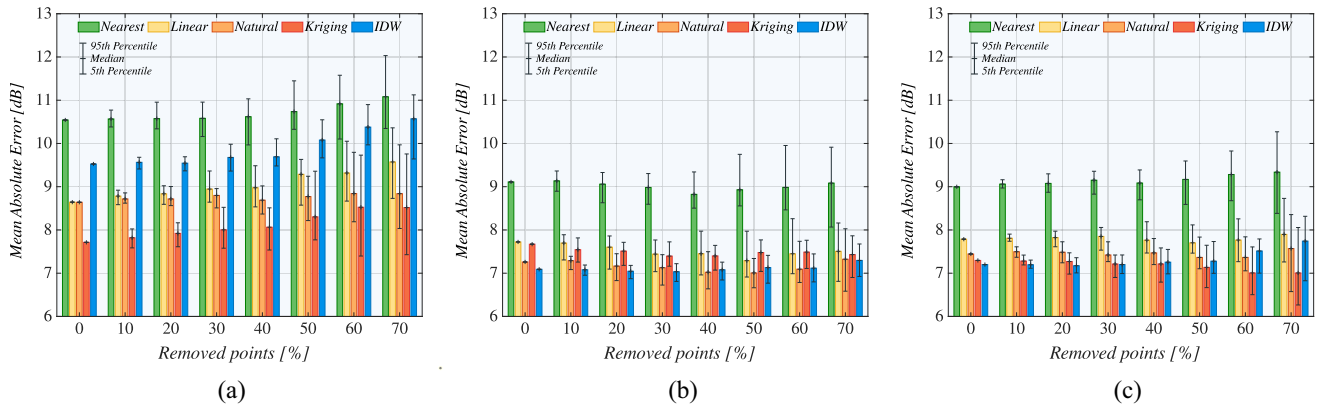


Fig. 9. Reference model comparison with interpolated data under deterministic thinning. (a) NB-IoT. (b) Sigfox. (c) LoRaWAN.

To this aim, Fig. 8 illustrates the coverage proportion with a given RSRP threshold as a function of the thinning algorithm in use, the type of the employed interpolation, and the number of the removed measurement points. Based on visual analysis, we focus on the NB-IoT technology, as it indicates the highest divergence among all the interpolation methods and reference models. For the sake of clarity, we also select only the two best-performing interpolation methods, i.e., Natural-neighbor and Kriging algorithms. Each subfigure contains the outcomes of 30 subsequent runs combining different thinning and interpolation algorithms. The resulting lines represent the median value based on all the repetitions while the translucent areas denote the 5th and 95th percentiles from left and right, respectively.

One of the essential observations based on the presented data is that the difference in the median values between the thinning algorithms is almost negligible for low numbers of the removed points, i.e., 10% (30 out of 300) and 30% (90 out of 300). However, probabilistic thinning is characterized by increased variance, thus resulting in a wider translucent area around the median curve. The difference is even more notable for higher numbers of the removed points, e.g., 70% (210 out of 300). Even though both thinning algorithms display significantly increased variance, the fluctuation for the deterministic algorithm remains two times smaller.

Surprisingly, the median value disparity between the thinning algorithms is lower for natural-neighbor interpolation,

whereas the Kriging method shows significant differences, especially for the RSRP values between -90 and -75 dBm. The Kriging variogram range most probably causes this fact, as it limits the sampling point impact on the interpolated value. Hence, with a more considerable distance between the sampling points, the Kriging option tends to produce bounded areas around the sampling points and settle on the average values in the rest of the plane. In practice, this implies that having a regular structure (such as a grid) for arranging an accurate assessment of the network coverage allows us to significantly decrease the resultant variance, especially for low numbers of the sampling points. Note that similar trends were observed for Sigfox and LoRaWAN deployments.

Furthermore, we report on the behavior of the MAE metric defined in (1), which captures the deviation from the reference models under probabilistic and deterministic thinning of the measurement points for all the considered LPWAN technologies and interpolation methods as illustrated in Figs. 9 and 10, respectively. As in the previous cases, the results summarize the output of 30 procedure runs, with the barplot head representing the median value and the error bars denoting the 5th and 95th percentiles. Based on the presented results, we may conclude that for the NB-IoT technology, the Kriging algorithm provides the closest approximation of the reference model under both probabilistic and deterministic thinning. Further analysis reveals that the median values for both thinning algorithms are almost identical. In several cases,

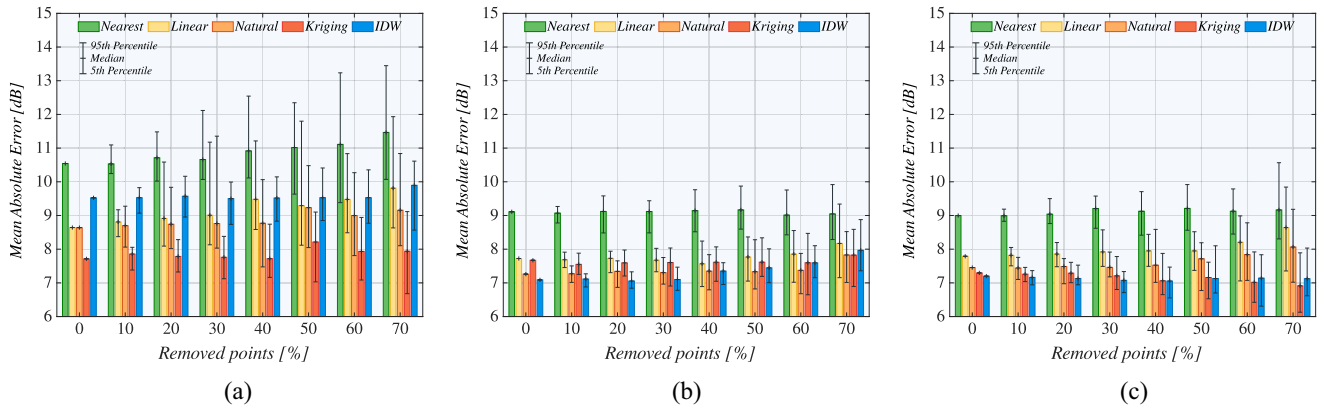


Fig. 10. Reference model comparison with interpolated data under probabilistic thinning. (a) NB-IoT. (b) Sigfox. (c) LoRaWAN.

probabilistic thinning provides even better results, albeit by a narrow margin (in the order of tenths of percents).

If we concentrate on the prediction variance, deterministic thinning provides more coherent results. Logically, this difference increases with higher number of the removed points. On average, probabilistic thinning variance is two times higher regardless of the interpolation algorithm. Hence, by selecting the deterministic algorithm, one can expect more predictable results, which can be slightly biased by the selection of the sampling point locations. This finding is most visible for the IDW interpolation with more than 50% of the removed points. In this case, probabilistic thinning provides a superior result over the deterministic algorithm. Since IDW predicts the values from the five closest neighboring points, there is a higher chance of clustering by nearby points when random thinning is applied. On the other hand, deterministic thinning tends to spread the sampling points more evenly; thus, the interpolation must select more distant neighbors with weaker mutual coherence.

Surprisingly, one can observe that IDW interpolation for Sigfox and LoRaWAN technologies under both thinning procedures leads to smaller differences between the considered models. For up to 40% of the removed points, IDW provides the closest approximation of the reference model for both LPWAN technologies and the considered thinning methods. In the case of Sigfox, for more than 50% of the removed points, the natural-neighbor interpolation leads to the best approximation. For LoRaWAN, the Kriging method offers the best approximation of the reference model for 40% and more points removed. This claim is valid for both deterministic and probabilistic thinning. Another conclusion from the coverage assessment accuracy is that the thinning method selection is not a crucial factor for sparse deployments. With six times sparser deployment of the Sigfox infrastructure as compared to the NB-IoT case, the 5th and 95th percentile variation under deterministic and probabilistic thinning is almost negligible. On the other hand, for the NB-IoT option, the deviation for probabilistic thinning is two times higher.

In summary, one can state these shared characteristics among the results depicted in Fig. 9 and Fig. 10. Clearly, decreasing the number of the measurement points leads to

a significantly higher variance in the MAE deviation, thus reducing statistical confidence in the obtained results. The mean deviation is higher for denser deployments represented by the NB-IoT technology. Furthermore, infrastructure density also influences the performance of thinning algorithms. For sparse deployments, the selected thinning method has a marginal impact on the resulting median and variation. The results also suggest that for sparse deployments, such as the ones in Sigfox and LoRaWAN networks, the IDW method provides the best approximation of the reference model for up to 40% of the removed points ($1.2 \text{ points per km}^2$). On the other hand, for dense cells (e.g., NB-IoT), it is the Kriging algorithm that shows the best approximation capabilities for all the cases of the removed points and thinning algorithms. For the downsides of the methods in question, simple Nearest-neighbor interpolation provides the worst approximation of the reference model in all situations. Finally, we note that the MAE deviation metric does not display any sharp increase across the entire range of the removed points from 10% ($1.8 \text{ points per km}^2$) to 70% ($0.6 \text{ points per km}^2$).

C. Lower Bound on Number of Measurements

Since the previous experiments did not identify any particular point where the MAE deviation from the reference model starts to vary significantly, we aimed to relaunch the procedure runs with 95% ($0.1 \text{ points per km}^2$) up to 99% ($0.02 \text{ points per km}^2$) of the removed points with the goal of producing a lower bound on the number of required measurements. To this end, Figs. 11 and 12 display the integral metric characterizing the absolute deviation for all the considered interpolation and thinning options.

For the NB-IoT technology, we can see similar characteristics of the thinning algorithms as in the case of Fig. 9 and Fig. 10. Deterministic thinning provides more consistent results than the probabilistic algorithm. Conversely, with the excessive number of removed points, the IDW method under deterministic thinning offers a better approximation of the reference model than the random case. For deterministic thinning, the IDW algorithm further represents the second best approximation, after the Kriging option. However, linear and natural-neighbor interpolations indicate more than two times

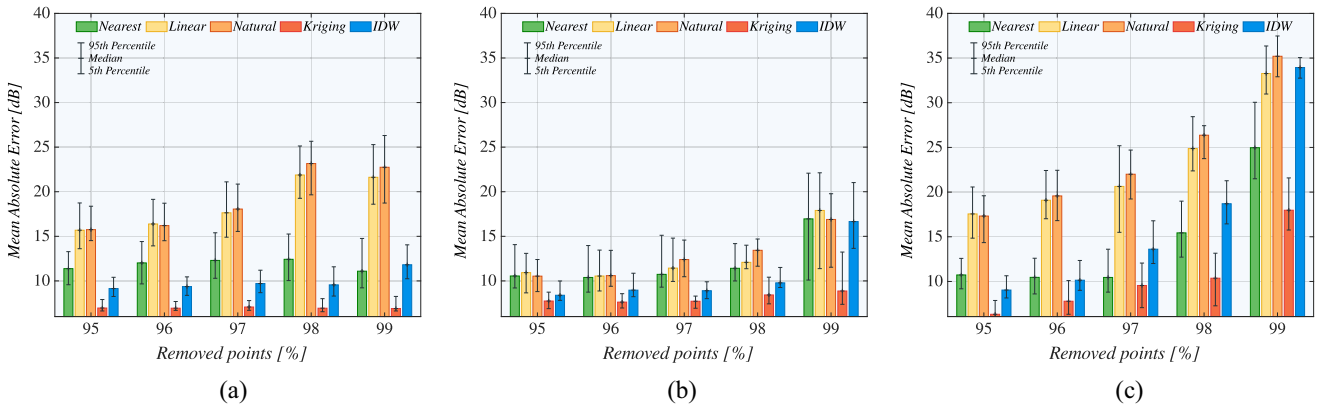


Fig. 11. Reference model comparison with interpolated data on lower bound of measurement points with deterministic thinning. (a) NB-IoT. (b) Sigfox. (c) LoRaWAN.

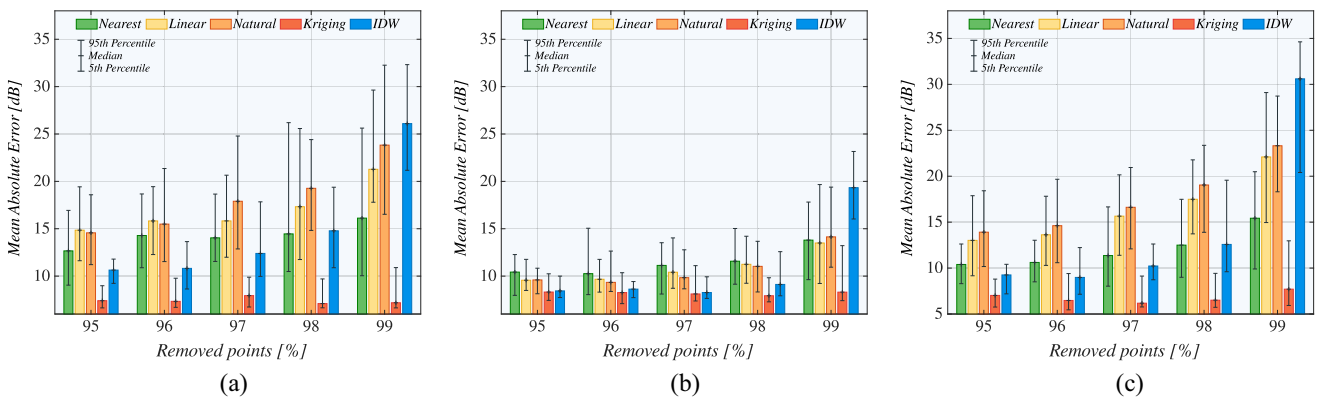


Fig. 12. Reference model comparison with interpolated data on lower bound of measurement points with random thinning. (a) NB-IoT. (b) Sigfox. (c) LoRaWAN.

higher mean deviation from the reference model as compared to the initial value (0% of the removed points).

Based on the above, the most promising findings are connected with the nearest-neighbor and Kriging algorithm. These methods display only a marginal increase in the mean deviation, even for 98% of the removed points. For the nearest-neighbor case, this means that the Voronoi diagram with a constant value in each polygon provides a better approximation of the reference model than for the Linear interpolation or the weighted average (Natural-neighbor). In the case of Kriging, the interpolation is solely influenced by the variogram range. If the points are separated by a distance larger than the variogram range, the Kriging method slowly settles to the median value of the samples.

A similar conclusion can be drawn for the LoRaWAN technology. In that case, the linear and natural-neighbor interpolations demonstrate the highest mean deviation from the reference model out of all the methods. Also, the Nearest-neighbor algorithm provides surprisingly consistent results. As in the previous cases, Sigfox features the most even results out of all the considered technologies. This further confirms that the deployment density significantly impacts the prediction accuracy. Finally, a deeper analysis of the results shows that the mean deviation peaks drastically for 98% or 99% of the removed points. However, that increase is due to the artificial

sample points, which then begin to severely influence the interpolation accuracy.

D. Accuracy Comparison With Measurement Data

At the last stage of our numerical evaluation, we compare the accuracy of the values predicted by both the reference model and the interpolation methods against the actual measurement results. This approach allows us to provide a convenient way of comparing the ground-truth data with the predicted values. In summary, with each step of the thinning procedure, the levels of the retracted points are compared to the values predicted by the interpolation algorithms and the reference model. This comparison uses the MAE metric defined in (1). Notably, only a comparison with the removed points is considered since the interpolation methods tend to retain the values of the generating points even for the predicted values. Hence, this would represent an unfair advantage for the interpolation methods if all the measurement points were considered.

A comparison of MAE for both thinning procedures, which is depicted in Figs. 13 and 14, confirms our earlier assumption that the deployment density influences the prediction accuracy. The NB-IoT technology with the highest BS density out of all the considered options features the increased MAE values by

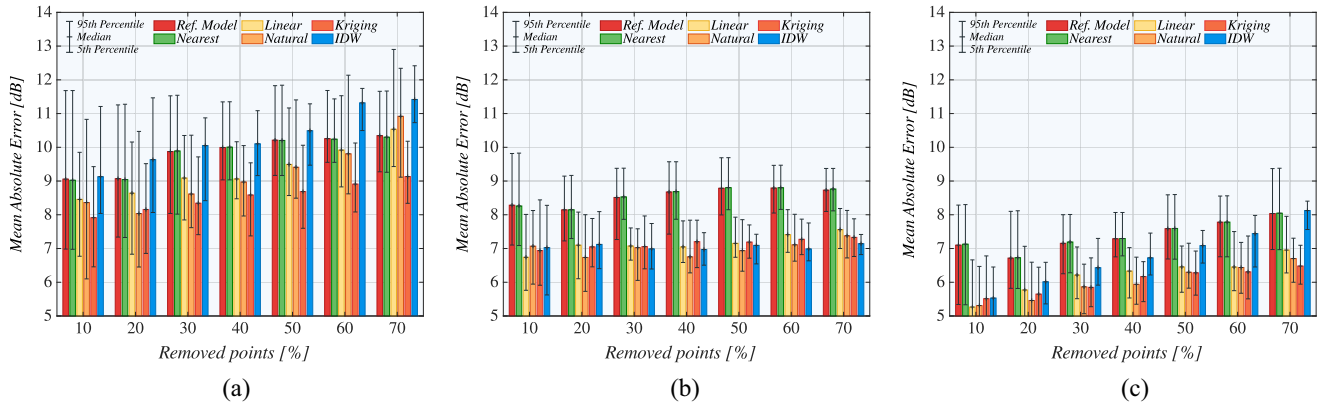


Fig. 13. Coverage accuracy assessment for interpolated data with deterministic thinning. (a) NB-IoT. (b) Sigfox. (c) LoRaWAN.

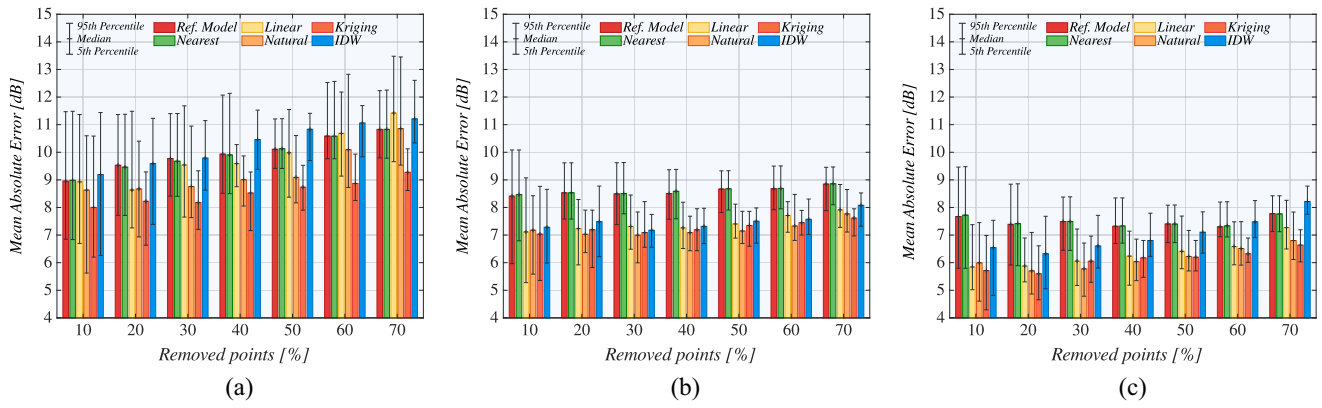


Fig. 14. Coverage accuracy assessment for interpolated data with probabilistic thinning. (a) NB-IoT. (b) Sigfox. (c) LoRaWAN.

2–3 dB on average. These findings are valid for both deterministic and probabilistic thinning. However, the most surprising outcome is related to the performance of the reference model. In most cases, the interpolation methods display notably better results than the fine-tuned propagation model. The two interpolation options that predict values less accurately are the simplest nearest-neighbor and the IDW. Furthermore, the only exception is the Sigfox technology, wherein the IDW performs satisfactorily, especially for deterministic thinning.

Conversely, the most versatile interpolation method is the Kriging algorithm, as it provides more accurate results independently of the selected technology, thinning procedure, or the number of retracted measurement points. Our results further indicate that the influence of the thinning methods is negligible. In contrast to the previous comparison with the reference model, the MAE is nearly identical for both deterministic and probabilistic thinning. Even the dispersion of the results is comparable for both approaches. The only exception from this rule is the LoRaWAN technology under deterministic thinning. In that case, MAE linearly increases with the number of retracted points. Notably, the MAE value is nearly constant for the remaining occasions from 10% (1.8 points per km^2) to 70% (0.6 points per km^2) of the removed points.

E. Lower Bound on Number of Measurements Points

The previous experiments did not reveal any particular point wherein MAE starts to deviate dramatically. Therefore,

we here consider the extreme cases of retracting from 95% (0.1 points per km^2) up to 99% (0.02 points per km^2) of points. To this end, our main goal is to discover a lower bound on the required number of the measurement points, which ensures accurate predictions. The results for the integral metric characterizing the absolute deviation for deterministic and probabilistic thinning methods are depicted in Figs. 15 and 16, respectively. These results reveal tremendous differences in the prediction accuracy for different LPWA technologies.

The outcomes for high-density NB-IoT deployments show almost two times higher MAE values in comparison to both Sigfox and LoRaWAN cases. Notably, this holds for both deterministic and probabilistic thinning. It is also evident that the Kriging method still holds the first place as the most accurate interpolation option even if compared to the reference model. Surprisingly, for NB-IoT and LoRaWAN, the linear and natural-neighbor interpolations display a notably increased prediction inaccuracy. For the extreme numbers of the removed points (98% and 99%), the presence of artificial “corner” points most probably causes this growth. However, for the lower numbers of the retracted points, the nature of these algorithms is responsible for that effect. In other words, the linear and natural-neighbor cases cannot adequately capture the geographical relations between far-away points. On the contrary, the Kriging method, which is specifically designed for this type of correlation, demonstrates its superiority.

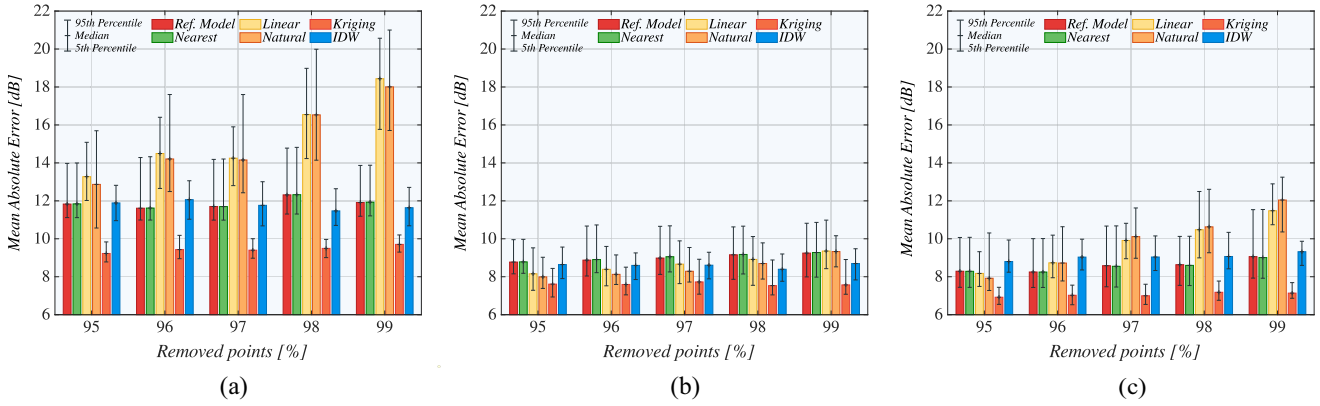


Fig. 15. Coverage accuracy assessment on lower bound of measurement points with deterministic thinning. (a) NB-IoT. (b) Sigfox. (c) LoRaWAN.

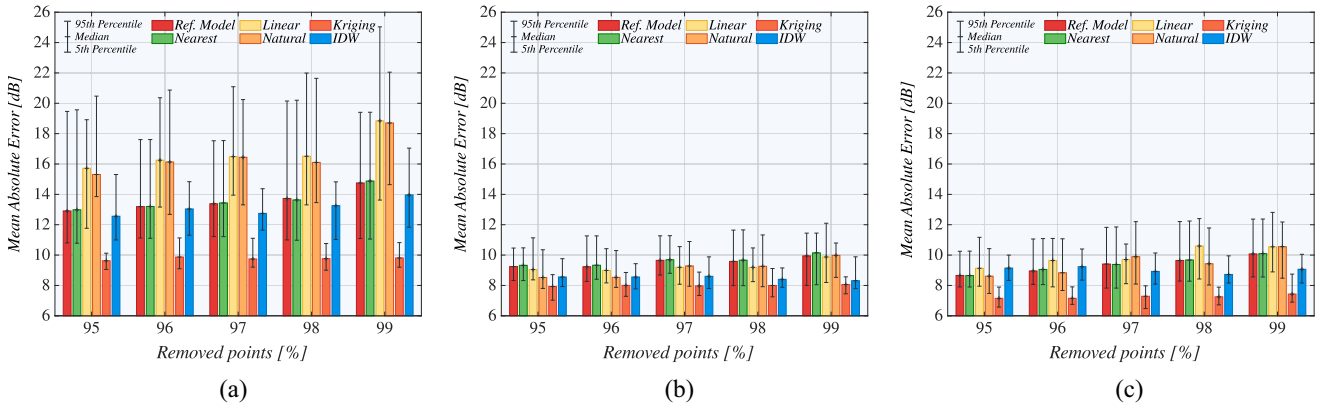


Fig. 16. Coverage accuracy assessment on lower bound of measurement points with probabilistic thinning. (a) NB-IoT. (b) Sigfox. (c) LoRaWAN.

VI. CONCLUSION

In this work, we approached the problem of coverage assessment in LPWAN deployments without explicit knowledge of the BS locations. This challenge may be typical for the potential customers who are willing to conduct an access network audit without direct involvement of the network provider. Also, as another example, the operators themselves can be willing to audit the performance of their network to update the layout or configuration. In our study, we primarily concentrated on the three most popular LPWAN technologies, for which the target consideration is particularly essential but the proposed methodology can also be applied to other wireless systems.

We systematically applied various interpolation algorithms to construct the key coverage assessment indicators without the knowledge of BS locations. As an alternative approach, the acquired measurement data can be used to infer the BS locations. This can be done by employing the conventional clusterization mechanisms, e.g., K -means, certain multilateration approaches, or more advanced algorithms based on machine learning. Additionally, we compared these results against the reference model produced by utilizing the experimental results with full BS location knowledge, see Section V for in-depth discussion.

Using the developed models, we demonstrated that the Kriging interpolation algorithm outperforms its counterparts

for NB-IoT deployments with significantly higher BS density. However, for sparser LoRaWAN and Sigfox infrastructures, the performance of simpler interpolation methods, including linear and natural-neighbor schemes, is comparable with that of the Kriging algorithm. The IDW technique is significantly more sensitive to the number of measurement points and does not produce accurate approximations in all of the cases. The accuracy of a signal quality assessment heavily depends on the coverage range of the considered radio technology, i.e., the required density of the BS locations. For the considered LPWAN technologies, we can conclude the averaged deviation for the reference model ranges around 8.5 dB in the case of NB-IoT and oscillates around 7.4 dB for Sigfox and LoRaWAN.

Notably, the higher is the density, the more significant is the deviation of the interpolation methods from the reference model. Furthermore, we concluded that random selection of the measurement points is as good as deterministic grid measurements. In practice, this implies that the choice of locations wherein measurements are to be made is not critical as long as they essentially cover the entire area of interest. Importantly, there is a limit on the number of measurement points where providing additional volumes of the spatial RSRP/RSSI data does not considerably improve the coverage assessment quality.

Going further, we report on the MAE deviation from the reference models under probabilistic and deterministic thinning,

i.e., the behavior of the defined integral metric. For the NB-IoT technology, the Kriging method displays the lowest deviation from the reference model in the case of both thinning procedures. However, if the focus is set on the prediction variance, deterministic thinning comes into play as it provides more coherent results. For Sigfox and LoRaWAN, one may observe dramatically lower MAE values when the IDW option is in use—it is a preferred choice in the scenario with up to 40% of the removed points. Most importantly, we highlight that the mean deviation metric does not demonstrate any sharp increase across the entire set of the removed points, ranging from 10% (1.8 points per km²) to 70% (0.6 points per km²).

Hence, we relaunch the procedure runs with 95% (0.1 points per km²) up to 99% (0.02 points per km²) of the removed points since the previous experiments (see Sections V-A and V-B) did not identify any specific evidence where the mean deviation starts to diverge significantly. While analyzing the provided results, one can see that the mean deviation increases for 98% or 99% of the removed points. This behavior is connected with the presence of artificial sample points, which at that time influence the interpolation precision.

Finally, we compare the accuracy of the generated models (reference and interpolated options with the measurement data representing the “ground truth”). The output suggests that the accuracy of the results is even less impacted by the selected thinning approach than in the previous cases. It is also evident that most of the employed interpolation methods perform better than the reference model. Particularly, the Kriging algorithm represents the most versatile option among all the interpolation methods, see Sections V-D and V-E. In the case of NB-IoT, the results indicate the highest MAE across all the selected LPWAN technologies, almost two times higher for more than 96% of the retracted points. These results verify our assumptions related to the fact that the deployment density influences the interpolation performance.

More generally, the telecommunication operators occasionally resort to optimistic coverage maps, which tend to present a better situation than what it actually is in the real-world conditions. Therefore, the end-customers often opt for their own field measurements to understand the current network performance. This approach becomes especially relevant with the development of automated measurement methodologies (e.g., drone-based) and crowdsourcing concepts (which can also be applied to machines). In these cases, there are essential benefits from the knowledge of the number of points required for an accurate signal and coverage assessment, which is delivered by the present research.

ACKNOWLEDGMENT

For this research, the infrastructure of the SIX Center was used.

REFERENCES

- [1] *Sigfox Connected Objects: Radio Specifications, Reference EP-SPECS, Revision 1.4*, Sigfox, Labège, France, Nov. 2019.
- [2] *LoRaWAN® 1.1 Specification*, LoRa Alliance®, Fremont, CA, USA, Oct. 2017.
- [3] A. Hoglund *et al.*, “Overview of 3GPP release 14 enhanced NB-IoT,” *IEEE Netw.*, vol. 31, no. 6, pp. 16–22, Nov./Dec. 2017.
- [4] U. M. Malik, M. A. Javed, S. Zezadly, and S. Ul Islam, “Energy efficient fog computing for 6G enabled massive IoT: Recent trends and future opportunities,” *IEEE Internet Things J.*, early access, Mar. 22, 2021, doi: [10.1109/JIOT.2021.3068056](https://doi.org/10.1109/JIOT.2021.3068056).
- [5] A. Shahrazi, M. Abbasi, M. J. Piran, and A. Taherkordi, “A comprehensive survey on 6G networks: Applications, core services, enabling technologies, and future challenges,” 2021. [Online]. Available: arXiv:2101.12475.
- [6] A. R. Mishra, *Fundamentals of Network Planning and Optimisation 2G/3G/4G: Evolution to 5G*. Hoboken, NJ, USA: Wiley, 2018.
- [7] J. T. Penttinen, *The LTE-Advanced Deployment Handbook: The Planning Guidelines for the Fourth Generation Networks*. Chichester, U.K.: Wiley, 2016.
- [8] M. J. Nawrocki, M. Dohler, and A. H. Aghvami, “Modern approaches to radio network modelling and planning,” *Understanding UMTS Radio Network Modelling, Planning and Automated Optimisation: Theory and Practice*. New York, NY, USA: Wiley, 2006, p. 3.
- [9] M. Stusek, D. Molchanov, P. Masek, J. Hosek, S. Andreev, and Y. Koucheryavy, “Learning-aided multi-RAT operation for battery lifetime extension in LPWAN systems,” in *Proc. 12th Int. Congr. Ultra Modern Telecommun. Control Syst. Workshops (ICUMT)*, 2020, pp. 26–32.
- [10] M. Stusek, D. Molchanov, P. Masek, S. Andreev, Y. Koucheryavy, and J. Hosek, “Time-dependent propagation analysis and modeling of LPWAN technologies,” in *Proc. IEEE Global Commun. Conf.*, Dec. 2020, pp. 1–7.
- [11] S. Puliti, L. T. Ene, T. Gobakken, and E. Næsset, “Use of partial-coverage UAV data in sampling for large scale forest inventories,” *Remote Sens. Environ.*, vol. 194, pp. 115–126, Jun. 2017.
- [12] B. S. Morse, C. H. Engh, and M. A. Goodrich, “UAV video coverage quality maps and prioritized indexing for wilderness search and rescue,” in *Proc. 5th ACM/IEEE Int. Conf. Human-Robot Interact.*, 2010, pp. 227–234.
- [13] S. M. Adams and C. J. Friedland, “A survey of unmanned aerial vehicle (UAV) usage for imagery collection in disaster research and management,” in *Proc. 9th Int. Workshop Remote Sens. Disaster Response*, vol. 8, 2011, pp. 1–8.
- [14] M. Brau, Y. Corre, and Y. Lostanlen, “Assessment of 3D network coverage performance from dense small-cell LTE,” in *Proc. IEEE Int. Conf. Commun. (ICC)*, 2012, pp. 6820–6824.
- [15] R. Amorim, H. Nguyen, P. Mogensen, I. Z. Kovács, J. Wigard, and T. B. Sørensen, “Radio channel modeling for UAV communication over cellular networks,” *IEEE Wireless Commun. Lett.*, vol. 6, no. 4, pp. 514–517, Aug. 2017.
- [16] M. Stusek *et al.*, “Accuracy assessment and cross-validation of LPWAN propagation models in urban scenarios,” *IEEE Access*, vol. 8, pp. 154625–154636, 2020.
- [17] P. Masek *et al.*, “Tailoring NB-IoT for mass market applications: A mobile operator’s perspective,” in *Proc. IEEE Globecom Workshops (GC Wkshps)*, 2018, pp. 1–7.
- [18] K. Mikhaylov *et al.*, “On the performance of multi-gateway LoRaWAN deployments: An experimental study,” in *Proc. IEEE Wireless Commun. Netw. Conf. (WCNC)*, 2020, pp. 1–6.
- [19] A. Gómez-Andrade, R. Barco, and I. Serrano, “A method of assessment of LTE coverage holes,” *EURASIP J. Wireless Commun. Netw.*, vol. 2016, no. 1, p. 236, Oct 2016. [Online]. Available: <https://doi.org/10.1186/s13638-016-0733-y>
- [20] M. Aernouts, R. Berkvens, K. Van Vlaenderen, and M. Weyn, “Sigfox and LoRaWAN datasets for fingerprint localization in large urban and rural areas,” *Data*, vol. 3, no. 2, p. 13, Apr. 2018. [Online]. Available: <http://dx.doi.org/10.3390/data3020013>
- [21] Y. Liu, W. Huangfu, H. Zhang, and K. Long, “Multi-criteria coverage map construction based on adaptive triangulation-induced interpolation for cellular networks,” *IEEE Access*, vol. 7, pp. 80767–80777, 2019.
- [22] M. Lauridsen, H. Nguyen, B. Vejlgaard, I. Z. Kovacs, P. Mogensen, and M. Sørensen, “Coverage comparison of GPRS, NB-IoT, LoRa, and SigFox in a 7800 km² Area,” in *Proc. IEEE 85th Veh. Technol. Conf. (VTC Spring)*, Jun. 2017, pp. 1–5.
- [23] R. V. Akhpashev and V. G. Drozdova, “Spatial interpolation of LTE measurements for minimization of drive tests,” in *Proc. 19th Int. Conf. Young Specialists Micro/Nanotechnol. Electron. Devices (EDM)*, Jun. 2018, pp. 6403–6405.
- [24] H. Braham, S. B. Jemaa, B. Sayrac, G. Fort, and E. Moulines, “Coverage mapping using spatial interpolation with field measurements,” in *Proc. IEEE 25th Annu. Int. Symp. Pers. Indoor Mobile Radio Commun. (PIMRC)*, Sep. 2014, pp. 1743–1747.

- [25] J. Talvitie, M. Renfors, and E. S. Lohan, "Distance-based interpolation and extrapolation methods for RSS-based localization with indoor wireless signals," *IEEE Trans. Veh. Technol.*, vol. 64, no. 4, pp. 1340–1353, Apr. 2015.
- [26] M. Chen, Y. Miao, X. Jian, X. Wang, and I. Humar, "Cognitive-LPWAN: Towards intelligent wireless services in hybrid low power wide area networks," *IEEE Trans. Green Commun. Netw.*, vol. 3, no. 2, pp. 409–417, Jun. 2019.
- [27] A. Laya, C. Kalalas, F. Vazquez-Gallego, L. Alonso, and J. Alonso-Zarate, "Goodbye, ALOHA!" *IEEE Access*, vol. 4, pp. 2029–2044, 2016.
- [28] O. Liberg, M. Sundberg, E. Wang, J. Bergman, J. Sachs, and G. Wikström, *Cellular Internet of Things: From Massive Deployments to Critical 5G Applications*. London, U.K.: Academic, 2019.
- [29] RP002-1.0.1® Regional Parameters, LoRa Alliance®, Beaverton, OR, USA, Feb. 2020.
- [30] Adeunis. *FTD: Network Tester*. Accessed: Jan. 14, 2019. [Online]. Available: <https://www.adeunis.com/>
- [31] U-Blox. *SARA-N2 Modules AT Commands Manual*. Accessed: Jan. 14, 2019. [Online]. Available: <https://www.u-blox.com/>
- [32] *GSM Penta Band Antenna*, document ANT-PCB8121, RF Solutions, Burgess Hill, U.K., Nov. 2011.
- [33] "LTE; Evolved universal terrestrial radio access (E-UTRA); Radio frequency (RF) system scenarios, version 15.0.0 release 15," 3GPP, Sophia Antipolis, France, Rep. TR 136 942, Jul. 2018.
- [34] *Interpolating Scattered Data—MATLAB & Simulink*, MathWorks, Natick, MA, USA, 2019. [Online]. Available: <https://uk.mathworks.com/help/matlab/math/interpolating-scattered-data.html>
- [35] P. Getreuer, "Linear methods for image interpolation," *Image Process. On Line*, vol. 1, pp. 238–259, Sep. 2011.
- [36] K. Hormann and N. Sukumar, *Generalized Barycentric Coordinates in Computer Graphics and Computational Mechanics*. Boca Raton, FL, USA: CRC Press, 2017.
- [37] Y. Diao, Z. Lin, and M. Fu, "A barycentric coordinate based distributed localization algorithm for sensor networks," *IEEE Trans. Signal Process.*, vol. 62, no. 18, pp. 4760–4771, Sep. 2014.
- [38] S. W. Park, L. Linsen, O. Kreylos, J. D. Owens, and B. Hamann, "Discrete Sibson interpolation," *IEEE Trans. Vis. Comput. Graphics*, vol. 12, no. 2, pp. 243–253, Mar./Apr. 2006.
- [39] R. Sibson, "A brief description of natural neighbor interpolation," in *Interpolating Multivariate Data*. New York, NY, USA: Wiley, 1981, pp. 21–36.
- [40] P. M. Bartier and C. Keller, "Multivariate interpolation to incorporate thematic surface data using inverse distance weighting (IDW)," *Comput. Geosci.*, vol. 22, no. 7, pp. 795–799, 1996.
- [41] D. Shepard, "A two-dimensional interpolation function for irregularly-spaced data," in *Proc. 23rd ACM Nat. Conf.*, 1968, pp. 517–524. [Online]. Available: <http://doi.acm.org/10.1145/800186.810616>
- [42] Q. Zhang and J. Wu, "Image super-resolution using windowed ordinary kriging interpolation," *Opt. Commun.*, vol. 336, pp. 140–145, Feb. 2015. [Online]. Available: <http://www.sciencedirect.com/science/article/pii/S003040181400889X>
- [43] A. McBratney and R. Webster, "Choosing functions for semi-variograms of soil properties and fitting them to sampling estimates," *J. Soil Sci.*, vol. 37, no. 4, pp. 617–639, 1986.
- [44] M. R. Inggs and R. T. Lord, "Interpolating satellite derived wind field data using ordinary kriging, with application to the nadir gap," *IEEE Trans. Geosci. Remote Sens.*, vol. 34, no. 1, pp. 250–256, Jan. 1996.



Martin Stusek received the B.Sc. and M.Sc. degrees in teleinformatics from Brno University of Technology (BUT), Brno, Czech Republic, in 2014 and 2016, respectively. He is currently pursuing the double Doctoral degrees with BUT and Tampere University, Tampere, Finland.

Since 2016, he has been working as a Researcher with the Wireless System Laboratory of Brno (WISLAB), Brno-Králové Pole, Czechia Republic. His research interests are in the area of wireless communication, with a focus on M2M, LPWAN technologies, 5G NR cellular networks, and device prototyping.



Dmitri Molchanov (Member, IEEE) received the M.Sc. and Cand.Sc. degrees from Saint Petersburg State University of Telecommunications, Saint Petersburg, Russia, in 2000 and 2003, respectively, and the Ph.D. degree from Tampere University of Technology, Tampere, Finland, in 2006.

He is currently a University Lecturer with the Laboratory of Electronics and Communications Engineering, Tampere University, Tampere. In his career, he has taught more than 50 full courses on wireless and wired networking technologies, the

P2P/IoT systems, network modeling, and queuing theory. He has (co)authored more than 150 publications on wireless communications, heterogeneous networking, IoT applications, and applied queuing theory. His current research interests include research and development of 5G/5G+ systems, ultrareliable low-latency service, the industrial IoT applications, mission-critical V2V/V2X systems, and blockchain technologies.



Pavel Masek (Member, IEEE) received the M.Sc. and Ph.D. degrees in electrical engineering from the Faculty of Electrical Engineering and Communication, Brno University of Technology (BUT), Brno, Czech Republic, in 2013 and 2017, respectively.

He is currently a Researcher with the Department of Telecommunications, BUT. He is also co-supervising the WISLAB Research Group, where his current interests include various aspects in the area of heterogeneous communication networks. He has coauthored more than 90 research works on a variety of networking-related topics in internationally recognized venues, including those published in the *IEEE Communications Magazine*, as well as several technology products.



Konstantin Mikhaylov (Senior Member, IEEE) received the Doctor of Technology degree from the University of Oulu, Oulu, Finland, in 2018.

He is currently the Assistant Professor of Convergent Wireless for IoT with the Centre for Wireless Communication, University of Oulu. In 2019, he has been a Visiting Research Fellow of the Brno University of Technology, Brno, Czech Republic, funded by the Ministry of Education, Youth and Sports of Czech Republic. He has authored and coauthored more than 70 research works on IoT wireless connectivity, system design, and applications.



Jiri Hosek (Senior Member, IEEE) received the M.Sc. and Ph.D. degrees in electrical engineering from the Faculty of Electrical Engineering and Communication, Brno University of Technology (BUT), Brno, Czech Republic, in 2007 and 2011, respectively.

He is currently an Associate Professor and the Deputy Vice-Head for Research and Development and International Relations with the Department of Telecommunications, BUT. He is also coordinating the WISLAB Research Group, where he deals mostly with industry-oriented projects in the area of future mobile networks, Internet of Things, and home automation services. He has coauthored more than 130 research works on networking technologies, wireless communications, quality of service, quality of experience, and IoT applications.



Sergey Andreev (Senior Member, IEEE) received the Specialist, Cand.Sc., and Dr.Habil. degrees from SUAI, Saint Petersburg, Russia, in 2006, 2009, 2019, respectively, and the Ph.D. degree from Tampere University of Technology, Tampere, Finland, in 2012.

He is an Associate Professor of Communications Engineering and an Academy Research Fellow of Tampere University.

He has been a Visiting Senior Research Fellow with King's College London, London, U.K., from 2018 to 2020, and a Visiting Postdoctoral Fellow of the University of California at Los Angeles, Los Angeles, CA, USA, from 2016 to 2017. He has coauthored more than 200 published research works on intelligent IoT, mobile communications, and heterogeneous networking.



Otto Zeman received the B.Sc. and M.Sc. degrees in teleinformatics from Brno University of Technology, Brno, Czech Republic, in 2006 and 2008, respectively.

He currently leads a team of IoT Solution Architect and IoT Service Architect, who support End-to-End (E2E) process of Vodafone IoT customers (presales, implementation and onboarding, acceptance, and service support) in Vodafone Czech.



Yevgeni Koucheryavy (Senior Member, IEEE) received the Ph.D. degree from Tampere University of Technology, Tampere, Finland, in 2004.

He is currently a Full Professor with Tampere University, Tampere. He has authored numerous publications in the field of advanced wired and wireless networking and communications. His current research interests include various aspects in heterogeneous wireless communication networks and systems, Internet of Things and its standardization, and nanocommunications.

Prof. Koucheryavy is an Associate Technical Editor of the *IEEE Communications Magazine* and an Editor of the *IEEE COMMUNICATIONS SURVEYS AND TUTORIALS*.



Pavel Kustarev received the M.Sc. and Cand.Sc. degrees from ITMO University, Saint Petersburg, Russia, in 1995 and 1999, respectively.

He is an Associate Professor with the Computer Science Department and the Head of Program Engineering and Computers Systems Faculty, Saint Petersburg National Research University of Information Technologies, Mechanics and Optics, ITMO University, Saint Petersburg, Russia. He was the Head of over ten Research and Development projects. He is a Supervisor for graduate and postgraduate students. He authored over 25 publications. His research interests include architectural design and analysis of systems-on-a-chip, networked embedded systems, and cyber-physical systems-based on wired and wireless networks.



Martin Roubicek received the B.Sc. and M.Sc. degrees in telecommunications engineering from Czech Technical University in Prague, Prague, Czech Republic, in 2002 and 2004, respectively.

He currently works as a Senior Radio Frequency System Engineer (RF planning and optimization) with Vodafone Czech.